

Ice Nucleating Properties of Glassy Organic and Organosulfate Aerosol

Christopher N. Rapp¹, Sining Niu², N. Cazimir Armstrong³, Xiaoli Shen¹, Thomas Berkemeier⁴, Jason D. Surratt^{3,5}, Yue Zhang², Daniel J. Cziczo¹

¹Department of Earth, Atmospheric and Planetary Sciences, Purdue University, West Lafayette, Indiana, 47906-2051, USA

²Department of Atmospheric Sciences, Texas A&M University, College Station, Texas, 77843-3150, USA

³Department of Environmental Sciences and Engineering, The University of North Carolina at Chapel Hill, Chapel Hill, North Carolina, 27599-7400, USA

⁴Multiphase Chemistry Department, Max Planck Institute for Chemistry, Mainz, 55128, Germany

⁵Department of Chemistry, The University of North Carolina at Chapel Hill, Chapel Hill, North Carolina, 27599-3290, USA

Correspondence to: Daniel J. Cziczo (djczczo@purdue.edu)

Abstract.

The role of secondary organic aerosol (SOA) in atmospheric ice nucleation is not well understood, limiting accurate predictions of aerosol-indirect effects in global climate simulations. This article details experiments performed to characterize the ice nucleating properties of proxy SOA. Experimental techniques in conditioning aerosol to glass transition temperatures (T_g) as low as -70°C using a pre-cooling unit are described. Ice nucleation measurements of proxy organosulfates (i.e., methyl, ethyl and dodecyl sulfates) and citric acid were performed using the SPectrometer for Ice Nucleation (SPIN) operating at conditions relevant to upper tropospheric cirrus temperatures (-45°C , -40°C , -35°C) and ice saturation ratios ($1.0 < S_{\text{ice}} < 1.6$). Methyl, ethyl, and dodecyl sulfates did not nucleate ice, despite dodecyl sulfate possessing a T_g higher than ambient temperature. Citric acid nucleated ice heterogeneously at -45 and -40°C ($1.2 < S_{\text{ice}} < 1.4$), but required pre-cooling temperatures of -70°C , notably colder than the lowest published T_g . A kinetic flux model was used to numerically estimate water diffusion timescales to verify experimental observations and predict aerosol phase state. Diffusion modeling showed rapid liquefaction of glassy methyl and ethyl sulfates due to high hygroscopicity, preventing heterogeneous ice nucleation. The modeling results suggest that citric acid nucleated ice heterogeneously via deposition freezing or immersion freezing after surface liquefaction. We conclude that T_g alone is not sufficient in predicting heterogeneous ice formation for proxy SOA using the SPIN.

1 Introduction

Aerosol-cloud interactions have profound effects on Earth's climate by modifying cloud properties such as formation, lifetime, radiative forcing, and precipitation (Albrecht, 1989; Hansen et al., 1997; Twomey, 1974). However, these interactions remain a large uncertainty in predicting future climate change (Myhre et al., 2014). Atmospheric ice nucleation contributes significantly to this uncertainty due to indirect radiative effects such as mixed-phase cloud glaciation (Knopf and Alpert, 2023; Lohmann and Feichter, 2005) and cirrus cloud formation (Gasparini et al., 2018; Hartmann et al., 2001). Ice nucleation also contributes significantly to the hydrological cycle through efficient ice initiated precipitation processes (Lau and Wu, 2003; Lohmann and Feichter, 2005). A more comprehensive understanding of atmospheric ice nucleation processes is critical in accurately estimating aerosol-cloud interactions and predicting their effects on the atmosphere and global climate.

Atmospheric ice formation occurs either homogeneously by spontaneously freezing solution droplets or heterogeneously by forming on ice nucleating particles (INPs) (Koop et al., 2000; Pruppacher and Klett, 1997). Aerosol particles such as mineral dust fulfill one of the traditional requirements of INPs; specifically, insolubility (i.e., a solid surface; Pruppacher and Klett, 1997; Vali et al., 2015). Secondary organic aerosol (SOA), or compounds selected as representative proxies, have demonstrated heterogeneous ice nucleation despite many being water soluble (Baustian et al., 2013; Ignatius et al., 2015; Kasparoglu et al., 2022; Kilchhofer et al., 2021; Murray et al., 2010; Schill et al., 2014; Schill and Tolbert, 2013; Wagner et al., 2010, 2012; Wang et al., 2012; Wilson et al., 2012; Wolf et al., 2020). This discrepancy is best explained by variations in aerosol phase state, where SOA in the atmosphere can exist as semisolid or a glass (Zobrist et al., 2008). A glass is formally defined by having a viscosity equal or higher than 10^{12} Pa s, but in the absence of direct viscosity measurements (Grayson et al., 2016; Song et al., 2015) the glass transition temperature (T_g) can be used to estimate the transition from a semi-solid to solid/glassy phase state (Koop et al., 2011). Determining T_g of atmospheric OAs is non-trivial and parameters such as relative humidity (RH), mixing state, hygroscopicity, molar mass, and atomic oxygen-to-carbon (O:C) ratio have all shown to affect T_g of complex aerosol mixtures (Derieux et al., 2017; Koop et al., 2011). These parameters also introduce complexity in experiments that control T_g as an experimental variable in ice nucleation studies, especially RH, a parameter difficult to measure at low temperatures.

Heterogeneous ice nucleation of SOA remains an active area of research (Knopf et al., 2018). Laboratory studies frequently conclude semisolid or glassy SOA require higher ice supersaturations to activate ice under cirrus conditions than mineral dust, i.e., they are comparatively poor INPs (Hoose and Möhler, 2012). Numerous studies have determined that SOA formed by the oxidation of select gas-phase precursors are homogeneous ice nuclei (Charnawskas et al., 2017; Ladino et al., 2014; Piedehierro et al., 2021; Prenni et al., 2009; Wagner et al., 2017), exhibiting onset conditions close to or above the homogeneous freezing threshold of aqueous droplets (Koop et al., 2000). A recent comprehensive study investigating the ice nucleating properties of SOA formed from eleven biogenic precursors reached a similar conclusion (Kasparoglu et al., 2022) and recommended both SOA and SOA-coated dust be treated as ice inactive entirely.

Despite SOA having lower ice active fractions and apparent departure from the traditional insolubility requirement of INPs, aircraft measurements have reported tropical subvisible cirrus ice residuals (IRs) are predominantly sulfate-organic in composition (Froyd et al., 2010). Moreover, the sulfate component of the IRs was highly neutralized, likely present as ammonium sulfate. This can result in phase-separated particles, where ice formation is initiated by crystalline ammonium sulfate submerged in an aqueous organic layer or by the glassy organic shell itself (Schill et al., 2014; Schill and Tolbert, 2013). For the IRs studied by Froyd et al., 2010 there was no statistically significant evidence that sulfate-rich particles preferentially nucleated ice, suggesting the organic component must also be ice active. This study is not an isolated example, numerous single particle mass spectrometry (Cziczo et al., 2004; Murphy et al., 1998, 2006, 2007) and bulk chemical composition measurements (Jimenez et al., 2009) have frequently discovered an abundance of tropospheric aerosol are organic. Evidence of these particles participating in cirrus formation in the atmosphere is also well documented by sampling IRs (Cziczo et al., 2013; Cziczo and Froyd, 2014; Froyd et al., 2009). It remains unclear whether the higher number density of SOA compensates for their poor ice nucleating efficiency.

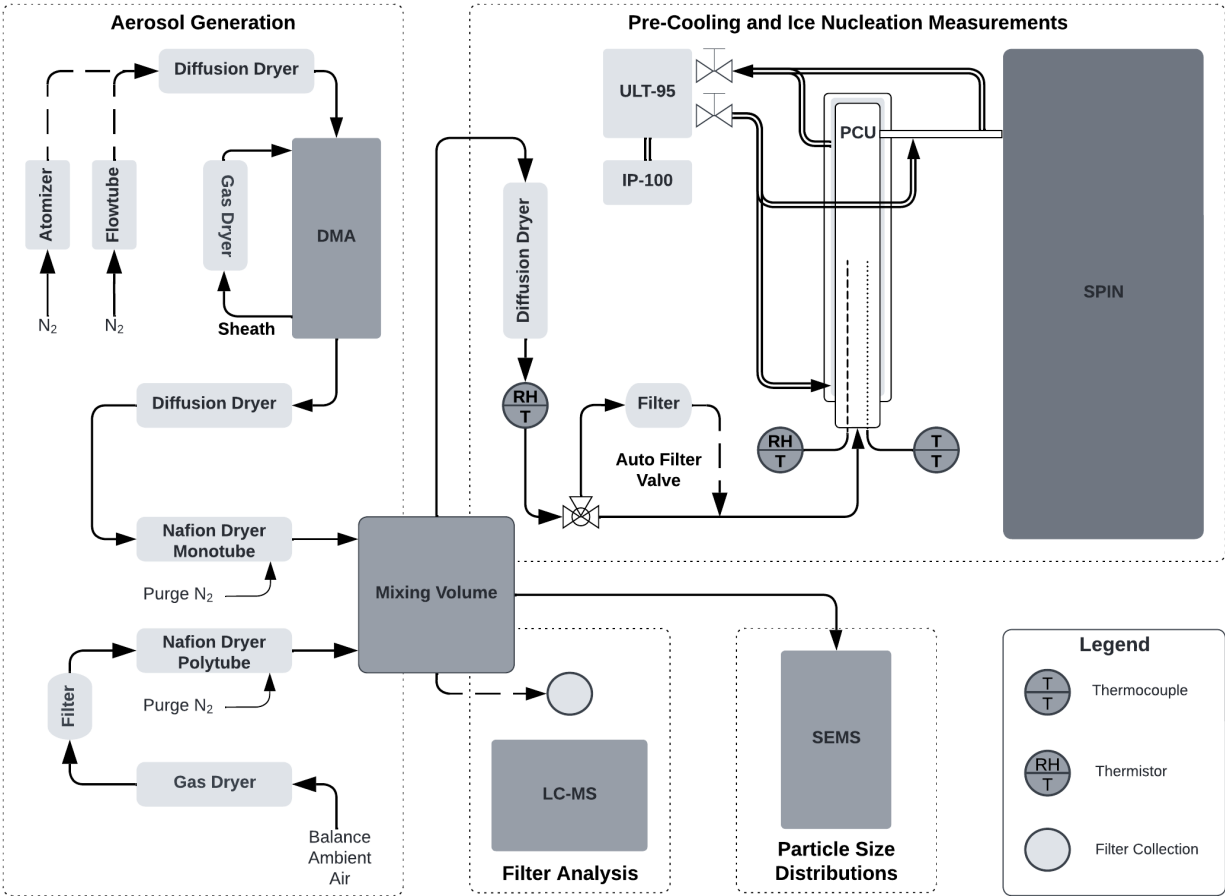
Mechanistically, both deposition and immersion freezing modes apply to SOA. For glassy aerosol, the current consensus is the deposition nucleation pathway occurs via active sites on the particle surface, a mechanism not possible for liquid particles. One proposed mechanism that describes how SOA serve as deposition INPs is an extension of the model for pore-condensational freezing (PCF) of mineral dust (Marcolli, 2014) or soot aggregates (Marcolli et al., 2021). SOA particles can exhibit similar morphology after ice cloud processing or “freeze-drying” (Adler et al., 2013; Wagner et al., 2017), where SOA droplets undergo homogeneous freezing then subsequent sublimation. This process forms a highly porous glassy surface structure, enhancing deposition ice nucleation (Wagner et al., 2012). Therefore, for SOA that have undergone atmospheric freeze-drying, depositional freezing of SOA can then be described analogously to the PCF model for mineral dust. Furthermore, evidence of immersion freezing has also been observed for glassy SOA where water uptake proceeds ice formation (Baustian et al., 2013). Phase-separated organic-sulfate aerosol have also demonstrated immersion freezing, where

85 water diffuses through the liquid organic shell to nucleate ice on crystalline ammonium sulfate “islands” within the simulated particle (Schill et al., 2014; Schill and Tolbert, 2013).

90 Experimental studies support the hypothesis that only SOA with a non-liquid phase state are heterogeneous INPs; however, much of the literature is limited to highly oxygenated model compounds used as proxy SOA such as citric acid (Kasparoglu et al., 2022; Murray et al., 2010), raffinose (Kilchhofer et al., 2021), or sucrose (Baustian et al., 2013). Studies of atmospherically relevant SOA are challenging as they require a combination of multidisciplinary laboratory techniques necessary to generate atmospherically relevant SOA from synthesized compounds or gas-phase precursors, constrain aerosol phase state, and measure ice nucleation properties.

95 The objectives of this study are to: (1) develop a pre-cooling technique to control the phase state of aerosol, (2) investigate the effects of different aerosol generation methods, (3) characterize the ice nucleating properties of proxy SOA and proxy SOA constituents, and (4) use water-diffusion modeling to evaluate our observations. Developing and characterizing this experimental framework is necessary for subsequent studies determining the ice nucleating properties of more atmospherically relevant SOA. Citric acid has demonstrated the ability to nucleate ice heterogeneously (Kasparoglu et al., 2022; Murray et al., 2010) and therefore was selected as a control compound for these experiments to validate the pre-cooling technique.
100 Additionally, methyl, ethyl, and dodecyl sulfate sodium salts were selected for investigation as proxy SOA constituents for organosulfates (OS), a type of SOA generated via acid-driven multiphase chemistry (Iinuma et al., 2007b, a; Riva et al., 2015, 2016; Surratt et al., 2007, 2008; Lin et al., 2012) that have been identified as potential heterogeneous ice nuclei in ambient measurements (Wolf et al., 2020). Both methyl and ethyl sulfate have been observed in ambient aerosol (Hettiyadura et al., 2017, 2019) using hydrophilic interaction liquid chromatography with MS detection (Hettiyadura et al., 2015). Dodecyl sulfate
105 has also been measured in ambient aerosols with possible formation processes linked to photochemical reactions of diesel fuel emissions with SO₂ (Blair et al., 2017). Previous studies have examined the hygroscopicity and cloud condensation nuclei (CCN) activity of these compounds as proxy OS (Estillore et al., 2016; Peng et al., 2021; Ruehl et al., 2010; Zhang et al., 2023); however, there is no literature describing their ice nucleating properties.

2 Methods



110 **Figure 1: Experimental schematic summarizing aerosol generation, particle size measurements, pre-cooling, filter collection, and ice**
115 **nucleation measurements. Alternate pathways for aerosol generation or filtering denoted by dashed line. See method sections for**
120 **full description of experimental design.**

2.1 Materials

For these experiments, we selected four commercially available compounds: (1) citric acid in both regular ($\geq 99.5\%$, 791725; Sigma-Aldrich) and anhydrous formulations ($\geq 99\%$, C0759; Sigma-Aldrich C0759), (2) methyl sulfate sodium salt (or methyl sulfate, $\geq 92\%$, 318183; Sigma-Aldrich), (3) ethyl sulfate sodium salt (or ethyl sulfate, $\geq 98\%$, 901275; Sigma-Aldrich), and (4) dodecyl sulfate sodium salt (or dodecyl sulfate, $\geq 95\%$, Sigma-Aldrich 8.22050). Diluted methanol solutions (MeOH, $\geq 99.8\%$, A412; Fisher Scientific) of the sodium salts were refrigerated until use. Additionally, control experiments included aqueous solutions of ammonium sulfate (AS, $\geq 99\%$, A4915; Sigma-Aldrich) and ammonium bisulfate (ABS, $\geq 99.99\%$, 455849; Sigma-Aldrich).

2.2 Experimental Temperatures

A pre-requirement for investigations of the ice nucleating properties of SOA is determining the range of temperatures and conditions at which glassy conditions may be met. For the purposes of this study, a glassy phase state is inferred by observing heterogeneous ice nucleation and/or maintaining a combination of temperature and RH below the T_g of each compound. SOA uptake water via hygroscopic growth under humid conditions, forming an organic-water mixture where water acts as a plasticizer (Koop et al., 2011). This water uptake due to RH effectively lowers the glass transition temperature of the pure “dry” organic ($T_{g,org}$) to that of the organic-water mixture T_g . The effect of RH on the T_g of SOA is explicitly defined using the Gordon-Taylor equation (Eq. 1), assuming the increase in humidity will form spherical aqueous solution droplets (Derieux et al., 2017; Gordon and Taylor, 1952; Koop et al., 2011):

$$T_g(w_{org}) = \frac{(1 - w_{org})T_{g,w} + \frac{1}{k_{GT}}w_{org}T_{g,org}}{(1 - w_{org})T_{g,w} + \frac{1}{k_{GT}}w_{org}}; \quad (1)$$

where $T_{g,w}$ is the glass transition temperature of water, k_{GT} is the Gordon-Taylor constant, w_{org} the organic mass fraction, and $T_{g,org}$ is the dry glass transition temperature of the organic component (Table 1). $T_{g,w}$ was defined as -137.15 ± 2 °C (Kohl et al., 2005) with a constant value of $k_{GT} = 2.5$ (Koop et al., 2011). To calculate w_{org} , the mass concentration of water (m_{H_2O}) and organic particles (m_{org}) are combined as a ratio (Eq. 2):

$$w_{org} = \frac{m_{org}}{m_{org} + m_{H_2O}}; \quad (2)$$

with m_{H_2O} represented by a parameterization of hygroscopic growth (Eq. 3) (Derieux et al., 2017) using the hygroscopicity parameter (κ) (Petters and Kreidenweis, 2007):

$$m_{H_2O} = \frac{\kappa \rho_w m_{org}}{\rho_{org} \left(\frac{1}{a_w} - 1 \right)}. \quad (3)$$

where density of water (ρ_w) was defined as 1 g cm^{-3} , ρ_{org} is 1.2 g cm^{-3} , and a_w is the water activity. For calculations of w_{org} , the following hygroscopicity parameters (κ) were selected: methyl sulfate [0.459 ± 0.021], (Peng et al., 2021); ethyl sulfate [0.397 ± 0.01], (Peng et al., 2021); dodecyl sulfate [0.135 ± 0.017], (Petters and Petters, 2016); and citric acid [0.233 ± 0.035], (Rickards et al., 2013).

Modeled values of $T_{g,org}$ for OS constituent proxies are calculated by their volatility (i.e., the saturation mass concentration), with semi-empirical fitting (Zhang et al., 2019). The vapor pressure is estimated from the melting and boiling temperatures (Myrdal and Yalkowsky, 1997). As boiling temperatures for the OS tested here are unknown, they were estimated using a group contribution model where each functional group in the compound possesses a group contribution value derived from fitting extensive experimental measurements of a large dataset of organic compounds (Ghasemitabar and Movagharnajad, 2016). For the selected compounds, we conducted experiments to simulate depositional ice nucleation relevant to upper tropospheric cirrus cloud formation (-45 °C to -35 °C). Previous studies operated the SPectrometer for Ice Nucleation (SPIN) at similar temperatures and ice supersaturations (S_{ice}) ($T = -46$ °C; $S_{ice} = 1.3$) to detect the ice nucleation of ambient isoprene SOA (Wolf et al., 2020).

Timescales of amorphous deliquescence (Mikhailov et al., 2009) were estimated using the kinetic multi-layer model of gas particle partitioning of aerosols and clouds (KM-GAP, Shiraiwa et al., 2012), generated with the kinetic multi-layer meta model generator (KM-MEMO, Berkemeier et al., in prep.). In the model, particles and their surrounding gas phase are discretized into concentric and spherical gas, surface and bulk layers. The model considers the relevant mass transport fluxes of water between these layers: gas diffusion, surface adsorption and desorption, surface-bulk transport, and bulk diffusion in the organic matrix. Diffusion of water between two bulk layers is calculated based on the water activity that corresponds to the average composition of the two layers. Layer numbers were increased until numerical convergence was achieved. The resulting system of ordinary differential equations was solved using Matlab software (ode23tb). The model utilizes temperature- and humidity-dependent parameterizations for the bulk diffusion coefficient of water in the organic matrix. For citric acid solutions, we used a detailed parameterization of aqueous citric acid density and water diffusivity (Lienhard et al., 2014), whereas for organosulfates, we relied on the method by (Berkemeier et al., 2014) to estimate diffusion coefficients based on glass transition temperatures and hygroscopicity parameters. The method modifies an existing Vogel-Fulcher-Tammann parameterization for the diffusivity of aqueous sucrose solutions at a given water activity (Zobrist et al., 2011) by changing the Vogel temperature to an estimate based on glass transition temperature.

The numerical model is set up to mimic the conditions in the SPIN chamber, which means that an individual model run is performed at constant temperature and RH. Particles entering the SPIN are assumed to be water-free, have a diameter of 0.225 μm , and glassy. For all four studied compounds, citric acid, methyl sulfate, ethyl sulfate and dodecyl sulfate, we explore a large range of possible experimental conditions, characterized by temperatures between $-65\text{ }^{\circ}\text{C}$ and $-25\text{ }^{\circ}\text{C}$ (in increments of 0.5 K) and S_{ice} between 0.8 and 1.7 (in increments of 0.01).

2.4 Aerosol Generation

OS proxies were atomized (Model 3076; TSI Inc., Shoreview, MN 3077) at a flow rate of 0.9 L min^{-1} using compressed zero grade air (Indiana Oxygen, Lafayette, IN). Each OS was dissolved in MeOH at a mass concentration of 1 mg/10 mL to match the lowest solubility of methyl sulfate in MeOH. MeOH was selected as the atomizing solvent to minimize water content in aerosol, and thus, limiting any potential hydrolysis of the OS proxies examined (Darer et al., 2011). Directly following atomization, an Erlenmeyer vacuum flask was positioned to trap any condensed liquid. Atomization of control inorganic sulfates were performed in an identical manner but as aqueous solutions.

Citric acid aerosol was generated using two techniques: (1) by atomizing citric acid in water at a mass ratio of 3.75 mg/10 mL in an identical manner as for the OS proxies and (2) thermal generation. Thermal generation was selected as an alternative to atomization to minimize aerosol liquid water content; MeOH atomization is not compatible with citric acid due to potential esterification (Rissman et al., 2007). Thermal generation was achieved by heating 1 g of citric acid in a custom 1.27 cm outer diameter glass flow tube with an ultra-high purity nitrogen carrier gas (UHP N_2 , Indiana Oxygen, Lafayette, IN) at a flow rate of 0.1 L min^{-1} . Resistive heating tape was wrapped around the flow tube with temperature controlled using a variable transformer (Type 3PN1010; Staco Energy Products) and monitored using a Type T thermocouple connected to a thermocouple calibrator (CL3512A, Omega Engineering). Immediately following the heated flow tube, a 5-L glass volume was placed to allow particle formation and growth via nucleation, condensation, and coagulation. All other aspects of particle generation mirror the atomization technique as shown in Figure 1.

To the best of our knowledge, thermal nucleation of citric acid aerosol has not been performed extensively, and we find conflicting literature surrounding the thermal behavior of citric acid. Melting (T_m) and initial decomposition temperatures (T_d) using differential scanning calorimetry (heating rate of $5\text{ }^{\circ}\text{C min}^{-1}$) for fine particles have been reported as $T_m = 153 \pm 0.2\text{ }^{\circ}\text{C}$, $T_d = 168\text{ }^{\circ}\text{C}$ (Barbooti and Al-Sammerrai, 1986) and $T_m = 160.8 \pm 0.2\text{ }^{\circ}\text{C}$, $T_d = 202.7\text{ }^{\circ}\text{C}$ (Reid et al., 2018), respectively. This large difference in temperatures is further complicated by a reported slow thermal decomposition beginning at $148\text{ }^{\circ}\text{C}$

205 (Barbooti and Al-Sammerrai, 1986). Initial experiments were conducted using a generating temperature of $\sim 160^\circ\text{C}$ with later experiments using temperatures below 148°C to avoid any potential thermal decomposition.

For atomization techniques, polydisperse aerosol was dried using a desiccant diffusion dryer and immediately size selected by a differential mobility analyzer (DMA, Model 3081A; TSI Inc., Shoreview, MN) to select $0.225\ \mu\text{m}$ diameter aerosol particles
210 operating at a (10:1) sheath to sample flow ratio. This electrical mobility mode was selected to minimize the transmission of doubly charged particles and maintain number concentrations of approximately $10^4\ \text{cm}^{-3}$. A desiccant gas drier was connected to the sheath flow of the electrostatic classifier (Model 3082; TSI Inc., Shoreview, MN) and maintained a RH of 5% throughout the entirety of each experiment. The monodisperse aerosol was then further dried using a diffusion dryer followed by a Nafion™ dryer (Model MD-700-12S-3; Perma Pure LLC, Lakewood, NJ) operating at a nitrogen (3:1) purge to sample flow.
215 Purge gas containing MeOH was disposed into a desiccant gas dryer. For thermal generation techniques all drying steps were identical; however, only polydisperse aerosol were sampled due to size selecting irregularities (see section 2.5). Immediately following all drying steps, aerosol was sampled into a 10-L mixing volume by each instrument to maintain stable concentrations throughout the experiment. Balance air provided to with ambient air was dried using a desiccant gas dryer and Nafion™ dryer (Model PD-50T-12MSS; Perma Pure LLC, Lakewood, NJ).

220 2.5 Particle Size Distributions

A scanning electrical mobility sizer (SEMS, Model 2002; Brechtel Manufacturing Inc., Hayward, CA) determined particle size distributions in 60 s intervals throughout the duration of the experiment and was operated at minimum sheath-to-flow ratio of 10. Sheath flow was dried using a desiccant gas dryer and resulting RH was less than 5% for all experiments. Sample flow was $0.25\text{--}0.3\ \text{L min}^{-1}$. Total number density was calculated for each size distribution and 1 Hz data points interpolated through
225 the experiment with a cubic spline using R software. Thermally generated citric acid aerosol exhibited irregular behavior when size selecting upstream, and we observed that the mode size was unstable due to static charging from the glass generation tube, varying by approximately $0.070\ \mu\text{m}$. Due to these problematic features, polydisperse thermally generated citric acid aerosol was used.

2.6 Pre-Cooling Unit (PCU)

230 We obtained sampling temperatures relevant to the T_g of our proxy SOA using a custom-built PCU (Fig. 1). The borosilicate chamber is a vacuum-jacketed flow tube (1.8×10^{-8} Torr) with an interior volume of 1 L and KF50 glass flange for inlet connections. Prior to entering the chamber, aerosol pass through a diffusion dryer and inline NTC humidity temperature transducer (HTM2500LF, TE Connectivity). Temperature and RH measurements within the chamber are obtained using both a Type T thermocouple and additional thermistor sealed into the PCU by a KF50 flange. Cooling was achieved with an ultra-
235 low temperature recirculating chiller (Neslab ULT-95; Thermo Fisher). Supplemental cooling was provided by inserting a low-temperature rigid coil probe (IP-100; PolyScience, Niles, Illinois) into the recirculating bath volume of the Neslab ULT-95. We used a high-performance thermal transfer silicone polymer (Syltherm™ XLT, Dow Chemical) as the working coolant for the system. After exiting the chamber, insulated conductive tubing connecting to the SPIN was also cooled to the same PCU chamber temperature to prevent sample warming prior to ice nucleation experiments.

240 Calibrations of the PCU were performed with a simulated SPIN sample flow of $0.85\ \text{L min}^{-1}$ UHP N_2 . The relationship between PCU temperature to chiller setpoint demonstrated a linear response. RH measurements are not included below a chamber temperature of -20°C . Repeated calibration experiments of UHP N_2 indicate this temperature limit is a more conservative threshold for accurate RH measurements in comparison to the manufacturer specified limit of -40°C . Manufacturer specified
245 uncertainties for low humidity applications (10 % or lower) are $\pm 5\%$ and are consistent with UHP N_2 calibration. Uncertainty for the chamber Type T thermocouple is $\pm 1^\circ\text{C}$ or $\pm 0.75\%$, whichever is greater. Sensors are interfaced using a microcontroller board (Arduino Mega) and retrieved using Python code with averaging performed to a sampling rate of 1 Hz.

2.7 Ice Nucleation Measurements

2.7.1 SPectrometer for Ice Nucleation (SPIN)

Ice nucleation activity of proxy SOA species were determined using the Spectrometer for Ice Nucleation (SPIN; Droplet Measurement Technologies, Longmont, CO). The SPIN is a continuous flow diffusion chamber (CFDC) that uses two flat parallel plates 1 cm apart (Garimella et al., 2016; Rogers, 1988; Wolf et al., 2019, 2021). During operation, each plate is coated with approximately 0.1 mm of ice, with temperature controlled by two independent refrigeration systems. Modifying temperatures of each iced plate results in both a temperature gradient and supersaturation gradient with respect to ice (Murphy and Koop, 2005). Aerosol are sampled into the chamber using a knife edge inlet and constrained to a laminar jet between two sheath flows with a maintained sheath-to-sample ratio of approximately 9:1. This design enables the confinement of aerosol within the lamina, allowing it to intersect a predetermined thermodynamic profile and simulate cloud conditions. Like other CFDC-style instruments, particles enter an isothermal evaporative segment immediately upon exiting the main chamber. In this evaporation section, the water vapor partial pressure is equivalent to the saturation vapor pressure over ice but subsaturated with respect to liquid, causing droplets to evaporate via the Bergeron–Wegener–Findeisen process (Pruppacher and Klett, 1997). Our experiments were conducted to simulate depositional ice nucleation relevant to upper tropospheric cirrus cloud formation (-45 °C, -40 °C, -35 °C; $1.0 < S_{ice} < 1.6$). These values were selected so conditions for water saturation, heterogeneous ice nucleation, and homogeneous ice nucleation of solution droplets could be observed. For each temperature, the lamina was kept isothermal throughout the chamber and S_{ice} increased from ice saturation to 1.6 at a rate of 0.015 min^{-1} for -45 °C and 0.024 min^{-1} otherwise. S_{ice} then decreased at the same rate back to ice saturation for each lamina temperature.

An optical particle counter (OPC) collected size (range of 0.5 to 15 μm), concentration, and scattering information on a particle-by-particle basis for aerosol exiting the droplet evaporation section of the SPIN chamber using four optical detectors (Garimella et al., 2016). Briefly, backscattering information is obtained using three detectors measuring the perpendicular (S_1) and parallel components (P_1 and P_2) of the polarized laser source. Backscattering optics for both S and P components have a detection angle of 135° and a half angle of 20° . Particle sizing is achieved using a side scatter detector which measures total scattering intensity. Particle size and concentration is recorded as both binned counts and, on a particle-by-particle basis as log-normalized intensity of side scattered light, reported here $\log_{10}(I_{size})$. The intensity counts obtained by each backscattering detector are used to calculate a depolarization ratio for individual particles and allows classification between aspherical and spherical particles (Nichman et al., 2016; Zenker et al., 2017). This is achieved by dividing the average intensities of the S and P detectors for the SPIN (Eq. 4) and normalized with bounds 0 and 1.

$$\delta_{\text{SPIN}} = \frac{\overline{S_i}}{\overline{P_i}} = \frac{2S_1}{P_1 + P_2} \quad (4)$$

Background frost released from the iced chamber walls was measured by sampling particle-free chamber air through an automatic filter valve upstream of the PCU. Frost counts were determined by summing particle counts larger than 2.5 μm for particle-free conditions and applying a five-minute smoothed linear interpolation across the experiment duration. To maintain conservative estimates of background frost, values were rounded up to the nearest whole number. Conversion to number density for all size data and background frost was performed using the volumetric chamber sample flow.

Accurate particle measurements assume sampled aerosol are constrained within the lamina; however, non-ideal ‘lamina spreading’ has been observed with continuous flow diffusion chambers such as the SPIN where aerosol positions extend beyond the lamina (DeMott et al., 2015; Garimella et al., 2017, 2018). These aerosol experience supersaturations less than required for activation and inadvertently lower the activated number density. Correction factors (CFs) to ice number density for the SPIN instrument range from 1.4 to 9.5 (Garimella et al., 2017). For this study we applied a conservative CF of 1.4 to all particle data.

2.7.2 Particle Classification and Onset Conditions

Traditionally, activated ice concentration for CFDC style instruments is determined by applying an instrument-specific size threshold (e.g. 2.5–5 μm) on post-evaporative optical particle data (Rogers et al., 2001). This technique is primarily limited by a phenomenon called water droplet breakthrough (WDBT), where droplets beyond a critical size will not evaporate to sizes below the size threshold used in classification. As described in the previous section, depolarization can be used to distinguish between aspherical (ice like) and spherical (droplet like) particles to mitigate WDBT and improve particle classification. In this study, particles were classified using a supervised machine learning (ML) approach combining chamber and particle data on an experiment-by-experiment basis.

First, preliminary classification was performed on particle data using empirically determined optical classification parameters δ_{SPIN} and $\log_{10}(I_{size})$ (see Sect. 2.7.1), following a similar procedure conducted by Garimella et al. (2016). These parameters were determined using known ice nucleating control compounds (AS and ABS) to generate five classes: aerosol, droplet, ice, water uptake, and unclassified. WDBT was observed for both AS and ABS at experimental temperatures of -35 °C. Homogeneous freezing of ABS aerosol corresponded to a distinct increase of δ_{SPIN} and plateaued above a δ_{SPIN} of 0.4. Heterogeneous freezing of AS coincided with a nearly identical profile of δ_{SPIN} . Unlike AS, ABS did not show ice formation below temperatures necessary for homogeneous freezing (i.e., -35 °C, see Sect. 3.1.1 for further detail). Droplet breakthrough of AS showed a distinct decrease in δ_{SPIN} as activated particles transitioned from the ice phase to droplets, with ABS shifting from a low δ_{SPIN} to about 0.2. Combining these observations, δ_{SPIN} values of 0.4 or 0.16 were used to first categorize data into ice, droplet, or aerosol/water uptake classes, respectively (see Figure 2). Aerosol/water uptake were grouped together on a δ_{SPIN} basis, but additional classification was performed using $\log_{10}(I_{size})$ and S_{liq} (see Table S1). Water uptake was a particularly important class for all organic aerosol examined (see Sect. 3.3). Unclassified aerosol was defined by particles not meeting the δ_{SPIN} and $\log_{10}(I_{size})$ classification criteria for any class.

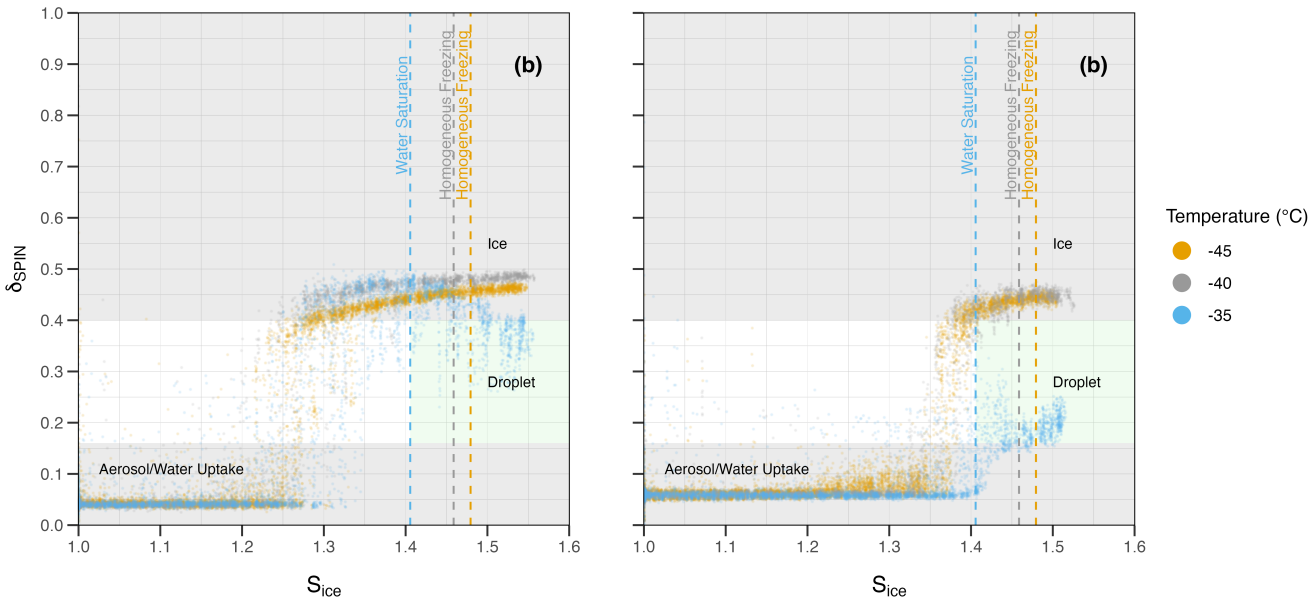


Figure 2: Optical scattering profiles obtained by the SPIN OPC for control experiments with 0.3 μm electrical mobility diameter ammonium sulfate (AS) panel (a) and ammonium bisulfate (ABS) panel (b) aerosol at three experiment lamina temperatures. Dashed lines correspond to experimental temperatures that correspond to homogeneous freezing (-40 °C and -45 °C, 0.3 μm diameter

aqueous solution droplets; Koop et al., 2000) or water saturation (-35 °C). Shaded regions indicate the estimated phase of aerosol exiting the SPIN chamber.

Following preliminary classification, supervised machine learning (ML) using a support vector machine (SVM) classifier was applied using the classification and regression training (caret) R package (Kuhn, 2008). The procedure consisted of the following steps: (1) generating a subset of SPIN experiment data with known particle type, (2) data partitioning, (3) data pre-processing, (4) SVM classifier training and cross-validation, and (5) application of model to uncategorized data. First, a subset of SPIN data was generated consisting of preliminary class (ice, droplet, water uptake), thermocouple measurements, calculated lamina values, flow rates, OPC size distribution data, and OPC particle-by-particle scattering data. Data partitioning was then performed to obtain a randomized 80:20 training to testing ratio of this data subset. Next, pre-processing was performed using principal component analysis (PCA) for dimension reduction and to lower computational cost. Approximately 11 principal components were selected that explained 95 % of the variance for each dataset. A SVM classifier with a radial basis function kernel was then applied to the training data. The performance of the classifier was evaluated with k-fold cross validation implemented with ten folds and was repeated three times to check for overfitting. Model accuracy was evaluated against the testing dataset. Finally, the highest performing model was applied to the original dataset to classify any uncategorized particles not captured by the preliminary classification described above. This classification technique was applied on an experiment-by-experiment basis i.e., citric acid at a PCU temperature of -70 °C was run separately from citric acid at a PCU temperature of 20 °C.

Activated fractions were obtained by dividing the background frost corrected number density of particles classified as ice by the interpolated total number density entering the chamber. For experiments using polydisperse citric acid, particles smaller than 0.1 µm were omitted from the total number density calculation and treated as ice inactive (Vali, 1966). Ice activation onset conditions for each experiment were defined as the first temperature and S_{ice} combination where particle activation fraction exceeded 0.5 %.

3 Results

Table 1: Summary of citric acid experiments performed. Columns from left to right indicate the following: tested compound, generation method, glass transition temperature of the pure organic, PCU chamber temperature, class of activated particles by the SPIN OPC, activation onset ice supersaturation for either ice nucleation or droplet breakthrough, onset temperature for either ice nucleation or droplet breakthrough, PCU chamber RH, inlet of PCU RH, geometric mean diameter of size distribution, geometric standard deviation of size distribution, and total particle concentration entering the SPIN. See Table S2 for all tabulated results.

Compound	Generation Method	$T_{g,org}$ (°C)	PCU Temperature (°C)	Class	Onset S_{ice}	Onset Temperature (°C)	PCU RH (%)	PCU Inlet RH (%)	D_{pg} (µm)	σ_g	CPC (n cm ⁻³)
citric acid, anhydrous	145 (°C), 0.1 L min ⁻¹	-13 ± 10	-70.4 ± 1.1	Ice	1.23 ± 0.08	-45 ± 0.4	-	0 ± 5	0.123	1.64	16909
citric acid, anhydrous	145 (°C), 0.1 L min ⁻¹	-13 ± 10	-70 ± 1.1	Ice	1.26 ± 0.08	-40 ± 0.4	-	0 ± 5	0.14	1.68	13586
citric acid	Atomizer	-13 ± 10	-65.7 ± 1.1	Ice	1.38 ± 0.1	-40 ± 0.4	-	0 ± 5	0.221	1.25	9572
citric acid	Atomizer	-13 ± 10	-65.7 ± 1.1	Ice	1.39 ± 0.1	-45 ± 0.4	-	0 ± 5	0.222	1.26	8692
citric acid, anhydrous	145 (°C), 0.1 L min ⁻¹	-13 ± 10	-70.3 ± 1.1	Droplet	1.48 ± 0.13	-35 ± 0.5	-	0 ± 5	0.167	1.73	11284

citric acid, anhydrous	140 (°C), 0.1 L min ⁻¹	-13 ± 10	-30 ± 1.1	Droplet	1.49 ± 0.13	-35 ± 0.5	-	0 ± 5	0.321	2	5806
citric acid	Atomizer	-13 ± 10	23.3 ± 1	Droplet	1.44 ± 0.13	-35 ± 0.5	0 ± 5	0 ± 5	0.204	1.3	14547
citric acid	Atomizer	-13 ± 10	23.4 ± 1	Droplet	1.5 ± 0.11	-40 ± 0.4	0 ± 5	0 ± 5	0.199	1.3	8955
citric acid	Atomizer	-13 ± 10	-65.9 ± 1.1	Droplet	1.52 ± 0.15	-35 ± 0.5	-	0 ± 5	0.22	1.24	12842
citric acid	Atomizer	-13 ± 10	23.2 ± 1	Droplet	1.57 ± 0.13	-46 ± 0.5	0 ± 5	0 ± 5	0.202	1.3	12045

3.1 Control Experiments

3.1.1 Sulfate Salts

350 ABS demonstrated homogeneous ice nucleation within the homogeneous freezing regime (Cziczko and Abbatt, 2001; Koop et al., 2000). Additionally, crystalline AS nucleated ice heterogeneously (Abbatt et al., 2006), and homogeneous freezing was not observed for the S_{ice} and temperatures tested. For ABS aerosol, droplet breakthrough and homogeneous freezing was proceeded by the onset of a feature classified as water uptake (see Table S2). In addition to the classification parameters described in Sect. 2.7.2, a distinct particle size increase from 0.3 μ m to 1.5 μ m for low S_{ice} (1–1.3) was observed. Ice activation onsets for ABS occurred at S_{ice} lower than the expected homogeneous freezing thresholds (see Fig. 2) due to a combination of measurement uncertainty in S_{ice} and neutralization of ABS to AS (Abbatt et al., 2006). This neutralization effect is particularly noticeable for post-calibration ABS measurements (see Table S2) where “aged” ABS (sampled several months later) resembled the ice onset conditions for crystalline AS.

3.1.2 Citric Acid

360 Results for citric acid experiments are summarized in Table 1 and illustrated in Fig. 3. For both atomization (citric acid) and thermal generation (citric acid, anhydrous) techniques, heterogeneous ice nucleation was observed only at the lowest attainable PCU temperatures (~ -70 °C) and required temperatures at or below -40 °C within the SPIN. Homogeneous freezing was not observed regardless of the generation technique or operating temperatures of the PCU. For experiments in which only droplet formation occurred, citric aerosol exhibited water uptake like ABS. Water uptake of citric acid generated via an atomizer exhibited a large variation in onset conditions with no discernable relationship. Notably, the onset of water uptake for anhydrous citric acid occurred at $S_{ice} \approx 1$ for all the SPIN temperatures examined (see section 5.3 for interpretation of this result).

3.2 Organosulfate (OS) Proxies

370 Model estimates of the $T_{g,org}$ for methyl, ethyl, and dodecyl sulfates were -83 ± 38 °C, -83 ± 34 °C, and 73.85 ± 13 °C respectively. Heterogeneous ice nucleation was not observed for any commercial OS proxy compounds tested for any PCU operating conditions. Droplet formation occurred at or above water saturation for all experimental temperatures (see Table S2 for compilation of OS proxy results) with a notable absence of homogeneous freezing (see discussion for interpretation of this result). For all OS proxy compounds, particle size increased prior to water saturation with a distinct increase in δ_{SPIN} to 0.15, which was stable until droplet formation was observed. The onset of this water uptake required higher S_{ice} for low temperature PCU operation (~ -70 °C) and was observed for both methyl and ethyl sulfates at all experimental temperatures. Additionally,

we found no evidence of any OS commercial standards being degraded by MeOH using RPLC/ESI-HR-QTOFMS analysis of filter samples (see supplement for additional details).

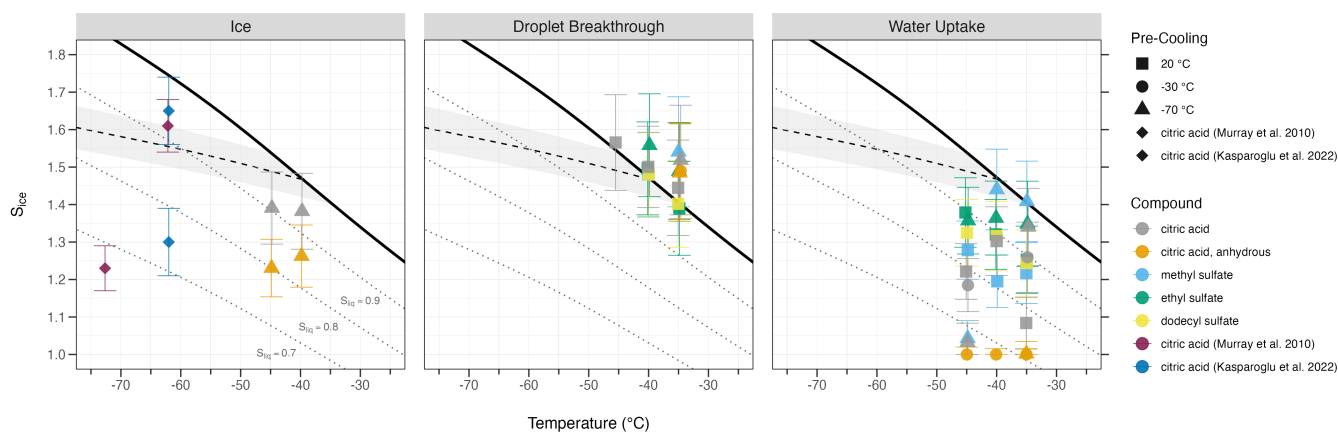


Figure 3: Thermodynamic onset conditions for ice, droplet breakthrough, and water uptake observed for all ice nucleation experiments conducted, including comparison to relevant literature. Shapes correspond to pre-cooling temperature setpoint or reported literature values. Black dashed line is the homogeneous freezing threshold of 0.1 μm diameter solution droplets (Koop et al., 2000) with shaded region indicating uncertainty in a_w of ± 0.025 (Koop, 2004). Solid black line is water saturation with dotted gray lines denoting equivalent lines of various liquid saturation ratios.

3.3 Liquefaction Timescales and Ice Nucleation Regimes

For each of the resulting model runs (7371 iterations to encompass conditions in the SPIN chamber), we derive characteristic timescales for the partial and full liquefaction of particles from the full model output. We define the partial liquefaction of particles (see discussion for analysis in the context of hygroscopic growth onset) as the point where particle volume has increased by more than 5 % due to water uptake. Full liquefaction is defined as the point where no model layer can be characterized as glassy anymore due to water uptake, i.e., the composition-dependent glass transition temperatures (Eq. 1) of each model layer is reduced below the chamber temperature. Table 2 shows a subset of the timescales for full liquefaction for $S_{\text{ice}} = 1$ and three different temperatures.

Table 2: Full liquefaction timescales (s) for selected temperatures and $S_{\text{ice}} = 1$ as determined by the numerical diffusion model. Empty cells indicate that full liquefaction did not occur in the simulations (up to 1000 s of experiment time).

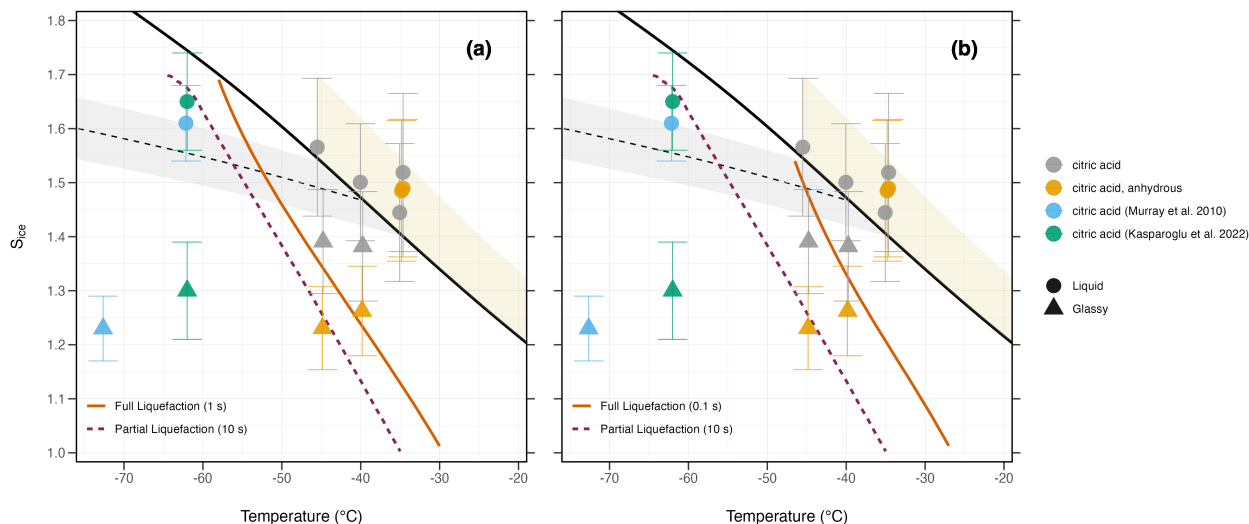
Temperature ($^{\circ}\text{C}$)	Citric Acid (s)	Dodecyl Sulfate (s)	Ethyl Sulfate (s)	Methyl Sulfate (s)
-45	-	-	0.215	0.185
-40	-	-	0.098	0.098
-35	145.8	-	0.055	0.060

For each temperature, we interpolate the model results to find the ice supersaturations at which (i) the full liquefaction timescale coincides with a characteristic residence time in the chamber of 10 s and (ii) the partial liquefaction timescale coincides with 12

395 a characteristic nucleation time of 0.1–1 s (Garimella et al., 2017). These sets of conditions represent the boundaries for three ice nucleation regimes (Berkemeier et al., 2014):

1. **Deposition Freezing** - If the partial liquefaction timescale is above the characteristic residence time (i.e., 10 s), particles do not take up water in the SPIN and thus can only nucleate ice in the deposition freezing mode.
- 400 2. **Homogeneous Freezing** - If the partial liquefaction timescale is below the characteristic nucleation time (i.e., 0.1–1 s), particles liquefy in the SPIN before heterogeneous freezing can occur and only nucleate ice in the homogeneous freezing mode.
3. **Immersion Freezing** - Between these boundaries, particles spend considerable time exhibiting a core-shell morphology in the SPIN and thus may be able to nucleate ice in the immersion freezing mode.

405 Among the compounds evaluated, only citric acid exhibits liquefaction timescales favorable for ice nucleation within the SPIN, as evident from a comparison of simulated liquefaction timescales and measured ice onsets of citric acid in Fig 4. The lowest temperature and humidity at which ice nucleation was observed for anhydrous citric acid (-45°C , $S_{\text{ice}} = 1.23$) coincides with the point at which the model suggests partial liquefaction to occur (dashed line in Fig. 4). The highest temperature and humidity at which ice nucleation was observed for anhydrous citric acid (-40°C , $S_{\text{ice}} = 1.26$) is at or near the point for which the model suggests full liquefaction to occur, depending on the assumed characteristic nucleation time of 1 s (Fig. 4a) or 0.1 s (Fig. 4b). We interpret such ice activation onsets between partial and full liquefaction conditions as immersion freezing. Dodecyl sulfate did not show significant water uptake at the temperatures and humidities for which ice nucleation could be expected, while methyl and ethyl sulfates equilibrated rapidly with the humidity in the SPIN, irrespective of temperature.



415 **Figure 4: Thermodynamic onset conditions for citric acid ice nucleation and relevant literature as well as humidity-induced phase transitions calculated with the diffusion model. Magenta colored line indicates the modeled partial liquefaction timescale (10 s characteristic residence time of the SPIN) where particle volume has increased by more than 5 % due to water uptake. Orange lines indicate two modeled full liquefaction timescales where citric acid is expected to be fully liquefied within 1 s (a) or 0.1 s (b) after entering the SPIN. Shapes correspond to aerosol phase state as reported in literature or defined using methods described above (e.g. PCU temperature lower than $T_{g,org}$ and ice nucleation observed below homogeneous freezing threshold). Black dashed line is the homogeneous freezing threshold of 0.1 μm diameter solution droplets (Koop et al., 2000) with shaded region indicating uncertainty in a_w of ± 0.025 (Koop, 2004). Solid black line is water saturation with dashed gray lines denoting equivalent lines of various liquid saturation ratios. Shaded yellow region indicates expected droplet breakthrough regime within the SPIN.**

4 Measurement Uncertainties

4.1 Glass Transition Temperature

Model estimations of $T_{g,org}$ for the selected OS proxies are based on their melting temperature, boiling temperature, and semi-empirical fitting. Unlike melting temperature, the boiling temperature for the OS proxies is not readily available and requires interpretation from their chemical composition. This process inherently introduces model uncertainties into the calculation for $T_{g,org}$. Furthermore, applying the Gordon-Taylor equation (Eq. 1) to calculate the T_g for binary mixtures combines model uncertainty with measured uncertainties in hygroscopicity parameter (κ) and RH. Uncertainties of the $T_{g,org}$ were calculated based on the procedure described in Section 2.2 and shown in Table 1. Experimentally, intrinsic instrument limitations exist for measuring RH at low temperatures. For example, chamber RH at dry conditions ($< 5\%$) is absent due to sensor limitations, leaving any inference in aerosol phase state dependent on whether ice nucleation was observed. Additionally, calibrations with high purity nitrogen have shown a high correlation between reported humidity and thermistor temperatures below $-20\text{ }^{\circ}\text{C}$, furthering the uncertainty when calculating T_g using measured chamber RH.

4.2 Ice Nucleation Measurements

Uncertainties in ice nucleation measurements for the SPIN instrument can be broadly defined as non-ideal lamina behavior, inhomogeneities of the chamber conditions, or particle detection in the OPC (Garimella et al., 2017). In this study, uncertainties in interpolated lamina position (Kulkarni and Kok, 2012) and chamber inhomogeneities were combined using propagation of errors (Taylor, 1997). The resulting uncertainty in lamina S_{ice} and temperature are calculated for every time interval during the experiment. Reported uncertainty for both onset temperature and S_{ice} are the calculated error at which the activation threshold was first met or exceeded. For this study, particle classification was performed using empirically derived parameters from compounds with known ice nucleating properties. An additional parameter used when distinguishing between droplets and ice is whether water saturation has been met. This introduces a bias only in the conditions we expect to observe droplet onset, not in classification of droplet breakthrough on a particle-by-particle basis.

5 Discussion

5.1 Implications of Aerosol Generation and Conditioning

Our results demonstrated that there are limitations in using T_g alone in predicting the heterogeneous ice nucleating properties of SOA proxies. Citric acid exhibited this for both generating techniques. First, atomizing citric acid solutions introduces a significant challenge in ice nucleation measurements as extreme drying techniques must be implemented to reduce the plasticizing effect of water (see Eq. 1). It has been estimated that at $5\text{ }^{\circ}\text{C}$ the sample RH must be below 10% to obtain glassy conditions (Kasparoglu et al., 2021). A study that successfully nucleated ice with citric acid utilized similar experimental methods which required extreme drying measures consisting of four diffusion dryers in series and a liquid N_2 trap (Kasparoglu et al., 2022). For all citric acid experiments performed (excluding the liquid citric acid experiments), PCU conditions were at or well below this threshold; however, heterogeneous ice nucleation was only observed at PCU temperatures near $-70\text{ }^{\circ}\text{C}$. Experiments conducted at $-30\text{ }^{\circ}\text{C}$, below the lowest published $T_{g,org}$ of citric acid ($-13 \pm 10\text{ }^{\circ}\text{C}$) (Murray, 2008), did not nucleate ice using atomization. These results were identical to thermally generating citric acid aerosol from anhydrous citric acid, despite being considered a dry technique for heating temperatures below the decomposition temperature (Barbooti and Al-Sammerrai, 1986; Wyrzykowski et al., 2011). Furthermore, predicting heterogeneous ice nucleation using T_g was unsuccessful for dodecyl sulfate, an OS proxy purposefully selected as a positive control due to a high $T_{g,org}$ of $74 \pm 13\text{ }^{\circ}\text{C}$. For a PCU RH of 5% (highest RH due to measurement error) the $T_{g(w_{org})}$ of dodecyl sulfate is $70.1 \pm 12.8\text{ }^{\circ}\text{C}$, much warmer than measured PCU temperature of $20.7 \pm 1\text{ }^{\circ}\text{C}$. This result, in addition to liquefaction timescales exceeding the particle residence time of SPIN, confirms that dodecyl sulfate remained glassy for all ice nucleation experiments.

465 Explanations for this inconsistency are not well understood but have been observed for atmospherically relevant biogenic SOA (Kasparoglu et al., 2022). Timescales in reaching equilibrium RH for certain SOA (Ingram et al., 2017) may not be sufficient for experimental designs with low residence times, which prevents a liquid to glass phase transition from occurring. Accuracy of RH measurements for experiments pre-cooling to low $T_{g,org}$ is also a source of uncertainty as encountered in these experiments, further obfuscating the expected phase state prior to testing ice nucleating properties. Even among effective INPs, 470 such as feldspars, the ice nucleating properties vary significantly. This was succinctly summarized as “not all feldspars are equal” by Harrison et al. (2016). Analogously, we attribute a similar characterization to SOA: not all glasses are equal.

5.2 Ice Nucleating Properties

Homogeneous freezing was not observed for any proxy SOA or proxy SOA constituents tested in this study, despite being observed for ABS using the same operating conditions in SPIN. Instead, droplet formation was frequently observed (Fig. 3) at 475 or above water saturation. This result is consistent with observations that organic material inhibit homogeneous freezing of aqueous solution droplets (Murray, 2008), requiring much higher S_{ice} than expected (Kasparoglu et al., 2022). Particles that activated as droplets in the SPIN exited the evaporation section with diameters $\geq 2.5 \mu m$, a size threshold frequently used to distinguish ice from droplets. We emphasize that using a traditional size cutoff was not a reliable method classify ice in these SPIN measurements.

480 Heterogeneous nucleation was only observed for citric acid aerosol conditioned to approximately $-70^\circ C$ (Table 1), indicating that the PCU was effective in inducing a glassy phase state. The onset temperature for both thermally and aqueously generated citric acid aerosol occurred at temperatures $\sim 20^\circ C$ warmer than found in the CSU-CFDC (Kasparoglu et al., 2022) or AIDA chamber (Murray et al., 2010), but at a similar onset S_{ice} (Fig. 3). Additionally, we observed the onset of heterogeneous ice 485 nucleation of citric acid required lower S_{ice} for thermally generated aerosol than aqueously generated. We theorize thermal generation of citric acid produces a glassy aerosol consisting of lower water content and thus a more viscous phase state. This would imply the aerosol population would contain increased activation site density (Vali et al., 2015) for particles. An additional factor that likely contributes to the lower onset conditions is the broader size distribution entering the SPIN since no size selection was conducted for this generation method due to static charging. This would lead to an increased total particle 490 surface area for thermally generated citric acid and consequently a higher number of activation sites.

The absence of heterogenous ice nucleation for both methyl and ethyl sulfates is consistent with particles exhibiting a liquid phase state. The lowest attainable PCU temperature was $-70^\circ C$, warmer than the $T_{g,org}$ of methyl and ethyl sulfates ($-83 \pm 38^\circ C$ and $-83 \pm 34^\circ C$, respectively). Furthermore, even if these particles obtained a glassy phase state, rapid particle liquefaction 495 would occur in the SPIN owing to their high hygroscopicity (Section 3.3), preventing the observation of heterogenous ice nucleation. The low $T_{g,org}$ of these OS proxy constituents is likely due to a lack of functionalization (e.g., hydroxyl, carboxyl, hydroperoxyl and carbonyl groups) that many other known atmospheric OS exhibit (Surratt et al., 2008, 2010). These additional functional groups significantly increase T_g (Zhang et al., 2019), in contrast to the proxy constituents tested which only contain one sulfate functional group. This limits our conclusions from broadly characterizing atmospheric OS as ice 500 inactive; moreover, our results supplement the finding of Wolf et al. (2020) that only highly functionalized OS are heterogeneous ice nuclei.

Studies that have recommended both SOA and SOA-coated dust be treated as ice inactive typically identify ice onset near or above the homogeneous freezing threshold of aqueous droplets (Kasparoglu et al., 2022; Koop et al., 2000). Furthermore, 505 Kasparoglu et al. (2022) argued that the onset conditions for experiments that have identified heterogeneous ice nucleation of SOA (Ignatius et al., 2015; Wang et al., 2012) may in fact be homogeneous freezing if a more restrictive parameterization of homogeneous freezing based on aqueous sulfuric acid droplets (Schneider et al., 2021) was applied. We caution that applying a sulfuric acid homogeneous freezing parameterization on SOA is of limited relevance due to the large difference in hygroscopicity. Biogenic SOA formed from various precursors or different oxidizing conditions in the laboratory setting are

510 less hygroscopic than sulfuric acid. Recently, a globally representative hygroscopicity parameter of organic aerosol systems (κ_{org}) was determined to be 0.12 ± 0.02 (Pöhlker et al., 2023). This is significantly less than that of sulfuric acid using either the growth factor ($\kappa = 1.19$) or CCN derived ($\kappa = 0.9$) form (Clegg et al., 1998; Petters and Kreidenweis, 2007).

5.3 Water Uptake and Particle Morphology

Experiments where proxy SOA only participated in droplet formation exhibited antecedent features classified as water uptake. In the absence of aerosol growth fraction measurements via a humidified tandem differential mobility analyzer, we are unable to conclusively refer to this water uptake as hygroscopic growth. Therefore, we cautiously suggest this rapid growth of particles from diameters $< 0.5 \mu\text{m}$ to $1.5 \mu\text{m}$ using the SPIN OPC is hygroscopic growth occurring within the SPIN chamber. We observed rapid particle growth for all proxy OS and citric acid. Similar features have been observed in experiments where longifolene and α -pinene SOA systems with and without sulfate uptake water at low S_{ice} (Charnawskas et al., 2017). The scattering profile obtained by the SPIN OPC for all organics that grew due to water uptake was nearly identical and distinct from the aerosol, ice and droplet classes identified using supervised ML. The onsets for water uptake varied among compounds and pre-cooling temperature. Anhydrous citric acid water uptake occurred immediately upon entering the SPIN ($S_{\text{ice}} \approx 1$). This result is expected as large particles from the polydisperse population produced during generation grew via water uptake to the detection limits of the SPIN OPC more readily than size selected particles. Citric acid experiments by atomization did not exhibit this feature, instead onset of water uptake varied greatly between PCU and SPIN temperatures. Water uptake for methyl and ethyl sulfates conditioned at or below $T_{\text{g,org}}$ using the PCU occurred at higher S_{ice} than those sampled at ambient temperature (Fig. 3). We propose this offset between onset of water uptake is related to decreased water diffusion for highly viscous or glassy particles (Berkemeier et al., 2014; Koop et al., 2011; Price et al., 2013; Zobrist et al., 2011).

Numerical diffusion modeling substantiates our observation of water uptake within the SPIN chamber and extends our results to infer the morphology of particles. Modeling results show that particle morphology upon rapid humidification as experienced in the SPIN shifts from an initial amorphous or semi-solid state towards full liquefaction. According to the diffusion model, methyl and ethyl sulfates are never glassy for more than a few milliseconds in the SPIN, which is consistent with the absence of heterogeneous ice nucleation. In contrast, dodecyl sulfate may not take up any water due to its high $T_{\text{g,org}}$ and comparably low hygroscopicity. Citric acid, on the other hand, has properties that favor the formation of core-shell morphologies in the temperature range -55 and -30°C , but this behavior is also highly dependent on ice supersaturation. Around -45 to -40°C , the core-shell morphology persists in the important range of S_{ice} between 1.3–1.4, where heterogeneous ice nucleation of glassy aerosols is typically observed. Thus, the ice nucleation observed in this study could involve immersion freezing on partially deliquesced glassy aerosols. This is consistent with observations that phase-separated organic-sulfate aerosol nucleate via immersion freezing, where sulfate islands nucleated ice despite being covered in a liquid organic layer (Schill and Tolbert, 2013).

6 Conclusions

Ice nucleation experiments were conducted at conditions relevant to upper tropospheric cirrus formation (-45°C , -40°C , -35°C ; $1.0 < S_{\text{ice}} < 1.6$) for proxy constituents of atmospheric SOAs. Generated aerosol was pre-cooled to conditions near or below their corresponding T_{g} to test the hypothesis that phase state of SOA influences heterogeneous ice nucleation. Primary conclusions of this study are as follows:

1. Ice nucleation of the proxy constituents of atmospheric OS examined are not heterogeneous ice nuclei in the temperature and supersaturation range considered here. We suggest that the sulfate functional group of OS aerosol itself is not critical to ice nucleation. Instead, the acid-catalyzed multi-phase chemistry driven by sulfate produces highly functionalized OS aerosol that are effective INPs as identified in ambient measurements.

2. Pre-cooling of dodecyl sulfate and citric acid below the estimated or published T_g (74 ± 13 °C and -13 ± 10 °C respectively) in the pre-cooling unit did not result in heterogeneous ice nucleation. From this, we conclude that T_g alone is not a sufficient condition for SOA to be considered INPs using the SPIN. Commonly, laboratory techniques using continuously generated aerosol to measure ice nucleating properties rely on using T_g as a metric to infer whether the aerosol phase is glassy, with confirmation of a glassy state being the detection of heterogeneous ice formation.
3. Diffusion modeling provides novel insight in the ice nucleation mechanisms for SOA and highlights experimental limitations when using CFDCs. Applied to the SPIN, we determined glassy particles liquefy within the instrument at certain timescales. Using diffusion modeling, we have determined the SPIN induces three conditions on glassy SOA: full liquefaction leading to deactivation, partial liquefaction requiring ice nucleation via immersion freezing, and deposition freezing when no liquefaction occurs.
4. Size thresholds used in traditional CFDC experiments to classify ice are insufficient in effectively characterizing the ice nucleating properties of SOA. We note an absence of any homogeneous freezing for proxy SOA experiments; rather, we observed evidence of water uptake preceding droplet formation as confirmed using scattering information from the SPIN OPC. Particles classified as droplets frequently exceeded the 2.5 μm size threshold, demonstrating a nominal size cutoff as being unreliable in quantifying the ice nucleating properties of SOA.

Despite many laboratory studies concluding SOA are broadly either entirely ineffective or even inhibitory to atmospheric ice formation, aircraft data has repeatedly confirmed a major fraction of cirrus cloud IRs contain organic matter (Froyd et al., 2010). Our measurements indicate that further experiments are needed to investigate ice nucleation of SOA, with careful consideration of aerosol generation techniques and efficacy of ice nucleation measurements. Ultimately, obtaining parameterizations necessary to fully capture the role of SOA in cirrus cloud formation requires further research investigating the interaction between aerosol phase state and heterogeneous ice nucleation of atmospherically relevant organic aerosol.

Code/Data availability

Code and data used in preparing this manuscript is available upon request of the corresponding author.

Author contribution

CR prepared the manuscript with contributions from all co-authors. CR performed all investigative experiments and data analysis. CR, SN, CA, and TB conducted formal analysis. CR and DC developed experimental methodology. CR, JS, YZ, and DC contributed to project conceptualization. JS, YZ, and DC acquired funding for the project.

Competing interests

Thomas Berkemeier and Jason Surratt are members of the editorial board of Atmospheric Chemistry and Physics.

Acknowledgments

The authors thank Smith, J. and the Jonathan Amy Facility for Chemical Instrumentation for fabricating the pre-cooling chamber.

Financial Support

600 This work was funded by the U.S. National Science Foundation under grant nos. AGS-2131369 (Zhang, PI), AGS-2131370
(Surratt, Co-PI), and AGS-2131371 (Cziczo, Co-PI).

605

- Abbatt, J. P. D., Benz, S., Cziczo, D. J., Kanji, Z., Lohmann, U., and Möhler, O.: Solid ammonium sulfate aerosols as ice nuclei: a pathway for cirrus cloud formation, *Science*, 313, 1770–1773, <https://doi.org/10.1126/science.1129726>, 2006.
- Adler, G., Koop, T., Haspel, C., Taraniuk, I., Moise, T., Koren, I., Heiblum, R. H., and Rudich, Y.: Formation of highly porous aerosol particles by atmospheric freeze-drying in ice clouds, *Proc. Natl. Acad. Sci.*, 110, 20414–20419, <https://doi.org/10.1073/pnas.1317209110>, 2013.
- Albrecht, B. A.: Aerosols, cloud microphysics, and fractional cloudiness, *Science*, 245, 1227–1230, <https://doi.org/10.1126/science.245.4923.1227>, 1989.
- Barbooti, M. M. and Al-Sammerrai, D. A.: Thermal decomposition of citric acid, *Thermochim. Acta*, 98, 119–126, [https://doi.org/10.1016/0040-6031\(86\)87081-2](https://doi.org/10.1016/0040-6031(86)87081-2), 1986.
- Baustian, K. J., Wise, M. E., Jensen, E. J., Schill, G. P., Freedman, M. A., and Tolbert, M. A.: State transformations and ice nucleation in amorphous (semi-)solid organic aerosol, *Atmos. Chem. Phys.*, 13, 5615–5628, <https://doi.org/10.5194/acp-13-5615-2013>, 2013.
- Berkemeier, T., Shiraiwa, M., Pöschl, U., and Koop, T.: Competition between water uptake and ice nucleation by glassy organic aerosol particles, *Atmos. Chem. Phys.*, 14, 12513–12531, <https://doi.org/10.5194/acp-14-12513-2014>, 2014.
- Blair, S. L., MacMillan, A. C., Drozd, G. T., Goldstein, A. H., Chu, R. K., Paša-Tolić, L., Shaw, J. B., Tolić, N., Lin, P., Laskin, J., Laskin, A., and Nizkorodov, S. A.: Molecular characterization of organosulfur compounds in biodiesel and diesel fuel secondary organic aerosol, *Environ. Sci. Technol.*, 51, 119–127, <https://doi.org/10.1021/acs.est.6b03304>, 2017.
- Charnawskas, J. C., Alpert, P. A., Lambe, A. T., Berkemeier, T., O’Brien, R. E., Massoli, P., Onasch, T. B., Shiraiwa, M., Moffet, R. C., Gilles, M. K., Davidovits, P., Worsnop, D. R., and Knopf, D. A.: Condensed-phase biogenic–anthropogenic interactions with implications for cold cloud formation, *Faraday Discuss.*, 200, 165–194, <https://doi.org/10.1039/C7FD00010C>, 2017.
- Clegg, S. L., Brimblecombe, P., and Wexler, A. S.: Thermodynamic model of the system $\text{H}^+ - \text{NH}_4^+ - \text{Na}^+ - \text{SO}_4^{2-} - \text{NO}_3^- - \text{Cl}^- - \text{H}_2\text{O}$ at 298.15 K, *J. Phys. Chem. A*, 102, 2155–2171, <https://doi.org/10.1021/jp973043j>, 1998.
- Cziczo, D. J. and Abbatt, J. P. D.: Ice nucleation in NH_4HSO_4 , NH_4NO_3 , and H_2SO_4 aqueous particles: implications for cirrus cloud formation, *Geophys. Res. Lett.*, 28, 963–966, <https://doi.org/10.1029/2000GL012568>, 2001.
- Cziczo, D. J. and Froyd, K. D.: Sampling the composition of cirrus ice residuals, *Atmos. Res.*, 142, 15–31, <https://doi.org/10.1016/j.atmosres.2013.06.012>, 2014.
- Cziczo, D. J., Murphy, D. M., Hudson, P. K., and Thomson, D. S.: Single particle measurements of the chemical composition of cirrus ice residue during CRYSTAL-FACE, *J. Geophys. Res.: Atmos.*, 109, 2003JD004032, <https://doi.org/10.1029/2003JD004032>, 2004.

- Cziczo, D. J., Froyd, K. D., Hoose, C., Jensen, E. J., Diao, M., Zondlo, M. A., Smith, J. B., Twohy, C. H., and Murphy, D. M.: Clarifying the dominant sources and mechanisms of cirrus cloud formation, *Science*, 340, 1320–1324, <https://doi.org/10.1126/science.1234145>, 2013.
- 645 Darer, A. I., Cole-Filipiak, N. C., O'Connor, A. E., and Elrod, M. J.: Formation and stability of atmospherically relevant isoprene-derived organosulfates and organonitrates, *Environ. Sci. Technol.*, 45, 1895–1902, <https://doi.org/10.1021/es103797z>, 2011.
- DeMott, P. J., Prenni, A. J., McMeeking, G. R., Sullivan, R. C., Petters, M. D., Tobo, Y., Niemand, M., Möhler, O., Snider, J. R., Wang, Z., and Kreidenweis, S. M.: Integrating laboratory and field data to quantify the immersion freezing ice
650 nucleation activity of mineral dust particles, *Atmos. Chem. Phys.*, 15, 393–409, <https://doi.org/10.5194/acp-15-393-2015>, 2015.
- Derieux, W. W., Li, Y., Lin, P., Laskin, J., Laskin, A., Bertram, A., Nizkorodov, S., and Shiraiwa, M.: Predicting the glass transition temperature and viscosity of secondary organic material using molecular composition, *Atmos. Chem. Phys.*, 18, 6331–6351, <https://doi.org/10.5194/ACP-18-6331-2018>, 2017.
- 655 Estillore, A. D., Hettiyadura, A. P. S., Qin, Z., Leckrone, E., Wombacher, B., Humphry, T., Stone, E. A., and Grassian, V. H.: Water uptake and hygroscopic growth of organosulfate aerosol, *Environ. Sci. Technol.*, 50, 4259–4268, <https://doi.org/10.1021/acs.est.5b05014>, 2016.
- Froyd, K. D., Murphy, D. M., Sanford, T. J., Thomson, D. S., Wilson, J. C., Pfister, L., and Lait, L.: Aerosol composition of the tropical upper troposphere, *Atmos. Chem. Phys.*, 9, 4363–4385, <https://doi.org/10.5194/acp-9-4363-2009>, 2009.
- 660 Froyd, K. D., Murphy, D. M., Lawson, P., Baumgardner, D., and Herman, R. L.: Aerosols that form subvisible cirrus at the tropical tropopause, *Atmos. Chem. Phys.*, 10, 209–218, <https://doi.org/10.5194/acp-10-209-2010>, 2010.
- Garimella, S., Kristensen, T. B., Ignatius, K., Welti, A., Voigtländer, J., Kulkarni, G. R., Sagan, F., Kok, G. L., Dorsey, J., Nichman, L., Rothenberg, D. A., Rösch, M., Kirchgäßner, A. C. R., Ladkin, R., Wex, H., Wilson, T. W., Ladino, L. A., Abbatt, J. P. D., Stetzer, O., Lohmann, U., Stratmann, F., and Cziczo, D. J.: The SPectrometer for ice nuclei (SPIN): an
665 instrument to investigate ice nucleation, *Atmos. Meas. Tech.*, 9, 2781–2795, <https://doi.org/10.5194/amt-9-2781-2016>, 2016.
- Garimella, S., Rothenberg, D. A., Wolf, M. J., David, R. O., Kanji, Z. A., Wang, C., Rösch, M., and Cziczo, D. J.: Uncertainty in counting ice nucleating particles with continuous flow diffusion chambers, *Atmos. Chem. Phys.*, 17, 10855–10864, <https://doi.org/10.5194/acp-17-10855-2017>, 2017.
- Garimella, S., Rothenberg, D. A., Wolf, M. J., Wang, C., and Cziczo, D. J.: How uncertainty in field measurements of ice
670 nucleating particles influences modeled cloud forcing, *J. Atmos. Sci.*, 75, 179–187, <https://doi.org/10.1175/JAS-D-17-0089.1>, 2018.
- Gasparini, B., Meyer, A., Neubauer, D., Münch, S., and Lohmann, U.: Cirrus cloud properties as seen by the *CALIPSO* satellite and ECHAM-HAM global climate model, *J. Clim.*, 31, 1983–2003, <https://doi.org/10.1175/JCLI-D-16-0608.1>, 2018.
- 675 Ghasemitabar, H. and Movagharnejad, K.: Estimation of the normal boiling point of organic compounds via a new group contribution method, *Fluid Phase Equilib.*, 411, 13–23, <https://doi.org/10.1016/j.fluid.2015.11.029>, 2016.

- Gordon, M. and Taylor, J. S.: Ideal copolymers and the second-order transitions of synthetic rubbers. i. non-crystalline copolymers, *J. Appl. Chem.*, 2, 493–500, <https://doi.org/10.1002/jctb.5010020901>, 1952.
- Grayson, J. W., Zhang, Y., Mutzel, A., Renbaum-Wolff, L., Böge, O., Kamal, S., Herrmann, H., Martin, S. T., and Bertram, A. K.: Effect of varying experimental conditions on the viscosity of α -pinene derived secondary organic material, *Atmos. Chem. Phys.*, 16, 6027–6040, <https://doi.org/10.5194/acp-16-6027-2016>, 2016.
- Hansen, J., Sato, M., and Ruedy, R.: Radiative forcing and climate response, *J. Geophys. Res.: Atmos.*, 102, 6831–6864, <https://doi.org/10.1029/96JD03436>, 1997.
- Harrison, A. D., Whale, T. F., Carpenter, M. A., Holden, M. A., Neve, L., O’Sullivan, D., Vergara Temprado, J., and Murray, B. J.: Not all feldspars are equal: a survey of ice nucleating properties across the feldspar group of minerals, *Atmos. Chem. Phys.*, 16, 10927–10940, <https://doi.org/10.5194/acp-16-10927-2016>, 2016.
- Hartmann, D. L., Holton, J. R., and Fu, Q.: The heat balance of the tropical tropopause, cirrus, and stratospheric dehydration, *Geophys. Res. Lett.*, 28, 1969–1972, <https://doi.org/10.1029/2000GL012833>, 2001.
- Hettiyadura, A. P. S., Stone, E. A., Kundu, S., Baker, Z., Geddes, E., Richards, K., and Humphry, T.: Determination of atmospheric organosulfates using HILIC chromatography with MS detection, *Atmos. Meas. Tech.*, 8, 2347–2358, <https://doi.org/10.5194/amt-8-2347-2015>, 2015.
- Hettiyadura, A. P. S., Jayarathne, T., Baumann, K., Goldstein, A. H., De Gouw, J. A., Koss, A., Keutsch, F. N., Skog, K., and Stone, E. A.: Qualitative and quantitative analysis of atmospheric organosulfates in centreville, alabama, *Atmos. Chem. Phys.*, 17, 1343–1359, <https://doi.org/10.5194/acp-17-1343-2017>, 2017.
- Hettiyadura, A. P. S., Al-Naiema, I. M., Hughes, D. D., Fang, T., and Stone, E. A.: Organosulfates in atlanta, georgia: anthropogenic influences on biogenic secondary organic aerosol formation, *Atmos. Chem. Phys.*, 19, 3191–3206, <https://doi.org/10.5194/acp-19-3191-2019>, 2019.
- Hoose, C. and Möhler, O.: Heterogeneous ice nucleation on atmospheric aerosols: a review of results from laboratory experiments, *Atmos. Chem. Phys.*, 12, 9817–9854, <https://doi.org/10.5194/ACP-12-9817-2012>, 2012.
- Ignatius, K., Kristensen, T., Järvinen, E., Niehman, L., Fuchs, C., Gordon, H., Herenz, P., Hoyle, C., Duplissy, J., Garimella, S., Dias, A., Frege, C., Höppel, N., Tröstl, J., Wagner, R., Yan, C., Amorim, A., Baltensperger, U., Curtius, J., Donahue, N., Gallagher, M., Kirkby, J., Kulmala, M., Möhler, O., Saathoff, H., Schnaiter, M., Tomé, A., Virtanen, A., Worsnop, D., and Stratmann, F.: Heterogeneous ice nucleation of viscous secondary organic aerosol produced from ozonolysis of α -pinene, *Atmos. Chem. Phys.*, 16, 6495–6509, <https://doi.org/10.5194/ACP-16-6495-2016>, 2015.
- Iinuma, Y., Müller, C., Berndt, T., Böge, O., Claeys, M., and Herrmann, H.: Evidence for the existence of organosulfates from β -pinene ozonolysis in ambient secondary organic aerosol, *Environ. Sci. Technol.*, 41, 6678–6683, <https://doi.org/10.1021/es070938t>, 2007a.
- Iinuma, Y., Müller, C., Böge, O., Gnauk, T., and Herrmann, H.: The formation of organic sulfate esters in the limonene ozonolysis secondary organic aerosol (SOA) under acidic conditions, *Atmos. Environ.*, 41, 5571–5583, <https://doi.org/10.1016/j.atmosenv.2007.03.007>, 2007b.

- Ingram, S., Cai, C., Song, Y.-C., Glowacki, D. R., Topping, D. O., O'Meara, S., and Reid, J. P.: Characterising the evaporation kinetics of water and semi-volatile organic compounds from viscous multicomponent organic aerosol particles, *Phys. Chem. Chem. Phys.*, 19, 31634–31646, <https://doi.org/10.1039/C7CP05172G>, 2017.
- 715 Jimenez, J., Canagaratna, M., Donahue, N., Prévôt, A., Zhang, Q., Kroll, J., DeCarlo, P., Allan, J., Coe, H., Ng, N., Aiken, A. C., Docherty, K., Ulbrich, I., Grieshop, A., Robinson, A., Duplissy, J., Smith, J. D., Wilson, K., Lanz, V., Hueglin, C., Sun, Y., Tian, J., Laaksonen, A., Raatikainen, T., Rautiainen, J., Vaattovaara, P., Ehn, M., Kulmala, M., Tomlinson, J., Collins, D. R., Cubison, M., Dunlea, J., Huffman, J. A., Onasch, T., Alfarra, M., Williams, P., Bower, K., Kondo, Y., Schneider, J., Drewnick, F., Borrmann, S., Weimer, S., Demerjian, K., Salcedo, D., Cottrell, L., Griffin, R., Takami, A., Miyoshi, T., Hatakeyama, S., Shimojo, A., Sun, J. Y., Zhang, Y. M., Džepina, K., Kimmel, J., Sueper, D., Jayne, J., Herndon, S., Trimborn, A., Williams, L., Wood, E., Middlebrook, A., Kolb, C., Baltensperger, U., and Worsnop, D.: Evolution of organic aerosols in the atmosphere, *Science*, 326, 1525–1529, <https://doi.org/10.1126/science.1180353>, 2009.
- 720 Kasparoglu, S., Li, Y., Shiraiwa, M., and Petters, M. D.: Toward closure between predicted and observed particle viscosity over a wide range of temperatures and relative humidity, *Atmos. Chem. Phys.*, 21, 1127–1141, <https://doi.org/10.5194/acp-21-1127-2021>, 2021.
- 725 Kasparoglu, S., Perkins, R., Ziemann, P. J., DeMott, P. J., Kreidenweis, S. M., Finewax, Z., Deming, B. L., DeVault, M. P., and Petters, M. D.: Experimental determination of the relationship between organic aerosol viscosity and ice nucleation at upper free tropospheric conditions, *J. Geophys. Res.: Atmos.*, 127, e2021JD036296, <https://doi.org/10.1029/2021JD036296>, 2022.
- 730 Kilchhofer, K., Mahrt, F., and Kanji, Z. A.: The role of cloud processing for the ice nucleating ability of organic aerosol and coal fly ash particles, *J. Geophys. Res.: Atmos.*, 126, e2020JD033338, <https://doi.org/10.1029/2020JD033338>, 2021.
- Knopf, D. A. and Alpert, P. A.: Atmospheric ice nucleation, *Nat. Rev. Phys.*, 5, 203–217, <https://doi.org/10.1038/s42254-023-00570-7>, 2023.
- Knopf, D. A., Alpert, P. A., and Wang, B.: The role of organic aerosol in atmospheric ice nucleation: a review, *ACS Earth Space Chem.*, 2, 168–202, <https://doi.org/10.1021/acsearthspacechem.7b00120>, 2018.
- 735 Kohl, I., Bachmann, L., Hallbrucker, A., Mayer, E., and Loerting, T.: Liquid-like relaxation in hyperquenched water at ≤ 140 K, *Phys. Chem. Chem. Phys.*, 7, 3210, <https://doi.org/10.1039/b507651j>, 2005.
- Koop, T.: Homogeneous ice nucleation in water and aqueous solutions, *Z. Phys. Chem.*, 218, 1231–1258, <https://doi.org/10.1524/zpch.218.11.1231.50812>, 2004.
- 740 Koop, T., Luo, B., Tsias, A., and Peter, T.: Water activity as the determinant for homogeneous ice nucleation in aqueous solutions, *Nature*, 406, 611–614, <https://doi.org/10.1038/35020537>, 2000.
- Koop, T., Bookhold, J., Shiraiwa, M., and Pöschl, U.: Glass transition and phase state of organic compounds: dependency on molecular properties and implications for secondary organic aerosols in the atmosphere, *Phys. Chem. Chem. Phys. : Pccp*, 13, 19238–55, <https://doi.org/10.1039/c1cp22617g>, 2011.
- 745 Kuhn, M.: Building predictive models in *R* using the **caret** package, *J. Stat. Softw.*, 28, <https://doi.org/10.18637/jss.v028.i05>, 2008.

Kulkarni, G. and Kok, G.: Mobile ice nucleus spectrometer, U.S. Department of Energy, Pacific Northwest National Laboratory, 2012.

Ladino, L. A., Zhou, S., Yakobi-Hancock, J. D., Aljawhary, D., and Abbatt, J. P. D.: Factors controlling the ice nucleating abilities of α -pinene SOA particles, *J. Geophys. Res.: Atmos.*, 119, 9041–9051, <https://doi.org/10.1002/2014JD021578>, 2014.

Lau, K. M. and Wu, H. T.: Warm rain processes over tropical oceans and climate implications, *Geophys. Res. Lett.*, 30, 2003GL018567, <https://doi.org/10.1029/2003GL018567>, 2003.

Lienhard, D. M., Huisman, A. J., Bones, D. L., Te, Y.-F., Luo, B. P., Krieger, U. K., and Reid, J. P.: Retrieving the translational diffusion coefficient of water from experiments on single levitated aerosol droplets, *Phys. Chem. Chem. Phys.*, 16, 16677, <https://doi.org/10.1039/C4CP01939C>, 2014.

Lin, P., Yu, J. Z., Engling, G., and Kalberer, M.: Organosulfates in humic-like substance fraction isolated from aerosols at seven locations in east Asia: a study by ultra-high-resolution mass spectrometry, *Environ. Sci. Technol.*, 46, 13118–13127, <https://doi.org/10.1021/es303570v>, 2012.

Lohmann, U. and Feichter, J.: Global indirect aerosol effects: a review, *Atmos. Chem. Phys.*, 2005.

Marcolli, C.: Deposition nucleation viewed as homogeneous or immersion freezing in pores and cavities, *Atmos. Chem. Phys.*, 14, 2071–2104, <https://doi.org/10.5194/acp-14-2071-2014>, 2014.

Marcolli, C., Mahrt, F., and Kärcher, B.: Soot PCF: pore condensation and freezing framework for soot aggregates, *Atmos. Chem. Phys.*, 21, 7791–7843, <https://doi.org/10.5194/acp-21-7791-2021>, 2021.

Mikhailov, E., Mikhailov, E., Vlasenko, S., Martin, S., Koop, T., and Pöschl, U.: Amorphous and crystalline aerosol particles interacting with water vapor: conceptual framework and experimental evidence for restructuring, phase transitions and kinetic limitations, *Atmos. Chem. Phys.*, 9, 9491–9522, <https://doi.org/10.5194/ACP-9-9491-2009>, 2009.

Murphy, D. M. and Koop, T.: Review of the vapour pressures of ice and supercooled water for atmospheric applications, *Q. J. R. Meteorolog. Soc.*, 131, 1539–1565, <https://doi.org/10.1256/qj.04.94>, 2005.

Murphy, D. M., Thomson, D. S., and Mahoney, M. J.: In situ measurements of organics, meteoritic material, mercury, and other elements in aerosols at 5 to 19 kilometers, *Science*, 282, 1664–1669, <https://doi.org/10.1126/science.282.5394.1664>, 1998.

Murphy, D. M., Cziczo, D. J., Froyd, K. D., Hudson, P. K., Matthew, B. M., Middlebrook, A. M., Peltier, R. E., Sullivan, A., Thomson, D. S., and Weber, R. J.: Single-particle mass spectrometry of tropospheric aerosol particles, *J. Geophys. Res.: Atmos.*, 111, 2006JD007340, <https://doi.org/10.1029/2006JD007340>, 2006.

Murphy, D. M., Cziczo, D. J., Hudson, P. K., and Thomson, D. S.: Carbonaceous material in aerosol particles in the lower stratosphere and tropopause region, *J. Geophys. Res.: Atmos.*, 112, 2006JD007297, <https://doi.org/10.1029/2006JD007297>, 2007.

Murray, B.: Inhibition of ice crystallisation in highly viscous aqueous organic acid droplets, *Atmos. Chem. Phys.*, 8, 5423–5433, <https://doi.org/10.5194/ACP-8-5423-2008>, 2008.

- 780 Murray, B. J., Wilson, T. W., Dobbie, S., Cui, Z., Al-Jumur, S. M. R. K., Möhler, O., Schnaiter, M., Wagner, R., Benz, S.,
Niemand, M., Saathoff, H., Ebert, V., Wagner, S., and Kärcher, B.: Heterogeneous nucleation of ice particles on glassy
aerosols under cirrus conditions, *Nat. Geosci.*, 3, 233–237, <https://doi.org/10.1038/ngeo817>, 2010.
- Myhre, G., Shindell, D., Bréon, F.-M., Collins, W., Fuglestad, J., Huang, J., Koch, D., Lamarque, J.-F., Lee, D., Mendoza,
B., Nakajima, T., Robock, A., Stephens, G., Zhang, H., Aamaas, B., Boucher, O., Dalsøren, S. B., Daniel, J. S., Forster, P.,
785 Granier, C., Haigh, J., Hodnebrog, Ø., Kaplan, J. O., Marston, G., Nielsen, C. J., O'Neill, B. C., Peters, G. P., Pongratz, J.,
Ramaswamy, V., Roth, R., Rotstayn, L., Smith, S. J., Stevenson, D., Vernier, J.-P., Wild, O., and Young, P.: Anthropogenic
and natural radiative forcing, in: *Climate Change 2013 – the Physical Science Basis: Working Group I Contribution to the
Fifth Assessment Report of the Intergovernmental Panel on Climate Change*, edited by: Jacob, D., Ravishankara, A. R., and
Shine, K., Cambridge University Press, Cambridge, 659–740, <https://doi.org/10.1017/CBO9781107415324.018>, 2014.
- 790 Myrdal, P. B. and Yalkowsky, S. H.: Estimating pure component vapor pressures of complex organic molecules, *Ind. Eng.
Chem. Res.*, 36, 2494–2499, <https://doi.org/10.1021/ie950242l>, 1997.
- Nichman, L., Fuchs, C., Järvinen, E., Ignatius, K., Höppel, N. F., Dias, A., Heinritzi, M., Simon, M., Tröstl, J., Wagner, A.
C., Wagner, R., Williamson, C., Yan, C., Connolly, P. J., Dorsey, J. R., Duplissy, J., Ehrhart, S., Frege, C., Gordon, H.,
Hoyle, C. R., Kristensen, T. B., Steiner, G., McPherson Donahue, N., Flagan, R., Gallagher, M. W., Kirkby, J., Möhler, O.,
795 Saathoff, H., Schnaiter, M., Stratmann, F., and Tomé, A.: Phase transition observations and discrimination of small cloud
particles by light polarization in expansion chamber experiments, *Atmos. Chem. Phys.*, 16, 3651–3664,
<https://doi.org/10.5194/acp-16-3651-2016>, 2016.
- Peng, C., Razafindrambina, P. N., Malek, K. A., Chen, L., Wang, W., Huang, R.-J., Zhang, Y., Ding, X., Ge, M., Wang,
X., Asa-Awuku, A. A., and Tang, M.: Interactions of organosulfates with water vapor under sub- and supersaturated
800 conditions, *Atmos. Chem. Phys.*, 21, 7135–7148, <https://doi.org/10.5194/acp-21-7135-2021>, 2021.
- Petters, M. D. and Kreidenweis, S. M.: A single parameter representation of hygroscopic growth and cloud condensation
nucleus activity, *Atmos. Chem. Phys.*, 7, 1961–1971, <https://doi.org/10.5194/acp-7-1961-2007>, 2007.
- Petters, S. S. and Petters, M. D.: Surfactant effect on cloud condensation nuclei for two-component internally mixed
aerosols, *J. Geophys. Res.: Atmos.*, 121, 1878–1895, <https://doi.org/10.1002/2015JD024090>, 2016.
- 805 Piedehierro, A. A., Welti, A., Buchholtz, A., Korhonen, K., Pullinen, I., Summanen, I., Virtanen, A., and Laaksonen, A.: Ice
nucleation on surrogates of boreal forest SOA particles: effect of water content and oxidative age,
<https://doi.org/10.5194/acp-2021-10>, 18 February 2021.
- Pöhlker, M. L., Pöhlker, C., Quaas, J., Mülmenstädt, J., Pozzer, A., Andreae, M. O., Artaxo, P., Block, K., Coe, H., Ervens,
B., Gallimore, P., Gaston, C. J., Gunthe, S. S., Henning, S., Herrmann, H., Krüger, O. O., McFiggans, G., Poulain, L., Raj, S.
810 S., Reyes-Villegas, E., Royer, H. M., Walter, D., Wang, Y., and Pöschl, U.: Global organic and inorganic aerosol
hygroscopicity and its effect on radiative forcing, *Nat. Commun.*, 14, 6139, <https://doi.org/10.1038/s41467-023-41695-8>,
2023.
- Prenni, A. J., Petters, M. D., Faulhaber, A., Carrico, C. M., Ziemann, P. J., Kreidenweis, S. M., and DeMott, P. J.:
Heterogeneous ice nucleation measurements of secondary organic aerosol generated from ozonolysis of alkenes, *Geophys.
815 Res. Lett.*, 36, 2008GL036957, <https://doi.org/10.1029/2008GL036957>, 2009.

- Price, H., Murray, B., Mattsson, J., O'Sullivan, D., Wilson, T. W., Baustian, K., and Benning, L.: Quantifying water diffusion in high-viscosity and glassy aqueous solutions using a raman isotope tracer method, *Atmos. Chem. Phys.*, 14, 3817–3830, <https://doi.org/10.5194/ACP-14-3817-2014>, 2013.
- 820 Pruppacher, H. R. and Klett, J. D.: *Microphysics of clouds and precipitation*, 2nd rev. and enl. ed., Kluwer Academic Publishers, Dordrecht ; Boston, 954 pp., 1997.
- Rickards, A. M. J., Miles, R. E. H., Davies, J. F., Marshall, F. H., and Reid, J. P.: Measurements of the sensitivity of aerosol hygroscopicity and the κ parameter to the O/C ratio, *J. Phys. Chem. A*, 117, 14120–14131, <https://doi.org/10.1021/jp407991n>, 2013.
- 825 Rissman, T. A., Varutbangkul, V., Surratt, J. D., Topping, D. O., McFiggans, G., Flagan, R. C., and Seinfeld, J. H.: Cloud condensation nucleus (CCN) behavior of organic aerosol particles generated by atomization of water and methanol solutions, *Atmos. Chem. Phys.*, 7, 2949–2971, <https://doi.org/10.5194/acp-7-2949-2007>, 2007.
- 830 Riva, M., Tomaz, S., Cui, T., Lin, Y.-H., Perraudin, E., Gold, A., Stone, E. A., Villenave, E., and Surratt, J. D.: Evidence for an unrecognized secondary anthropogenic source of organosulfates and sulfonates: gas-phase oxidation of polycyclic aromatic hydrocarbons in the presence of sulfate aerosol, *Environ. Sci. Technol.*, 49, 6654–6664, <https://doi.org/10.1021/acs.est.5b00836>, 2015.
- Riva, M., Da Silva Barbosa, T., Lin, Y.-H., Stone, E. A., Gold, A., and Surratt, J. D.: Chemical characterization of organosulfates in secondary organic aerosol derived from the photooxidation of alkanes, *Atmos. Chem. Phys.*, 16, 11001–11018, <https://doi.org/10.5194/acp-16-11001-2016>, 2016.
- 835 Rogers, D. C.: Development of a continuous flow thermal gradient diffusion chamber for ice nucleation studies, *Atmos. Res.*, 22, 149–181, [https://doi.org/10.1016/0169-8095\(88\)90005-1](https://doi.org/10.1016/0169-8095(88)90005-1), 1988.
- Rogers, D. C., DeMott, P. J., Kreidenweis, S. M., and Chen, Y.: A continuous-flow diffusion chamber for airborne measurements of ice nuclei, *J. Atmos. Oceanic Technol.*, 18, 725–741, [https://doi.org/10.1175/1520-0426\(2001\)018<0725:ACFDCE>2.0.CO;2](https://doi.org/10.1175/1520-0426(2001)018<0725:ACFDCE>2.0.CO;2), 2001.
- 840 Ruehl, C. R., Chuang, P. Y., and Nenes, A.: Aerosol hygroscopicity at high (99 to 100%) relative humidities, *Atmos. Chem. Phys.*, 10, 1329–1344, <https://doi.org/10.5194/acp-10-1329-2010>, 2010.
- Schill, G., Haan, D. O. D., and Tolbert, M.: Heterogeneous ice nucleation on simulated secondary organic aerosol, *Environ. Sci. Technol.*, 48 3, 1675–82, <https://doi.org/10.1021/es4046428>, 2014.
- Schill, G. P. and Tolbert, M. A.: Heterogeneous ice nucleation on phase-separated organic-sulfate particles: effect of liquid vs. glassy coatings, *Atmos. Chem. Phys.*, 13, 4681–4695, <https://doi.org/10.5194/acp-13-4681-2013>, 2013.
- 845 Schneider, J., Höhler, K., Wagner, R., Saathoff, H., Schnaiter, M., Schorr, T., Steinke, I., Benz, S., Baumgartner, M., Rolf, C., Krämer, M., Leisner, T., and Möhler, O.: High homogeneous freezing onsets of sulfuric acid aerosol at cirrus temperatures, *Atmos. Chem. Phys.*, 21, 14403–14425, <https://doi.org/10.5194/acp-21-14403-2021>, 2021.
- 850 Shiraiwa, M., Pfrang, C., Koop, T., and Pöschl, U.: Kinetic multi-layer model of gas-particle interactions in aerosols and clouds (KM-GAP): linking condensation, evaporation and chemical reactions of organics, oxidants and water, *Atmos. Chem. Phys.*, 12, 2777–2794, <https://doi.org/10.5194/acp-12-2777-2012>, 2012.

- Song, M., Liu, P., Hanna, S., Li, Y., Martin, S., and Bertram, A.: Relative humidity-dependent viscosities of isoprene-derived secondary organic material and atmospheric implications for isoprene-dominant forests, *Atmos. Chem. Phys.*, 15, 5145–5159, <https://doi.org/10.5194/ACP-15-5145-2015>, 2015.
- 855 Surratt, J. D., Lewandowski, M., Offenberg, J. H., Jaoui, M., Kleindienst, T. E., Edney, E. O., and Seinfeld, J. H.: Effect of acidity on secondary organic aerosol formation from isoprene, *Environ. Sci. Technol.*, 41, 5363–5369, <https://doi.org/10.1021/es0704176>, 2007.
- 860 Surratt, J. D., Gómez-González, Y., Chan, A. W. H., Vermeylen, R., Shahgholi, M., Kleindienst, T. E., Edney, E. O., Offenberg, J. H., Lewandowski, M., Jaoui, M., Maenhaut, W., Claeys, M., Flagan, R. C., and Seinfeld, J. H.: Organosulfate formation in biogenic secondary organic aerosol, *J. Phys. Chem. A*, 112, 8345–8378, <https://doi.org/10.1021/jp802310p>, 2008.
- Surratt, J. D., Chan, A. W. H., Eddingsaas, N. C., Chan, M., Loza, C. L., Kwan, A. J., Hersey, S. P., Flagan, R. C., Wennberg, P. O., and Seinfeld, J. H.: Reactive intermediates revealed in secondary organic aerosol formation from isoprene, *Proc. Natl. Acad. Sci.*, 107, 6640–6645, <https://doi.org/10.1073/pnas.0911114107>, 2010.
- 865 Taylor, J. R.: An introduction to error analysis: the study of uncertainties in physical measurements, 2. ed., University Science Books, Sausalito, Calif, 327 pp., 1997.
- Twomey, S.: Pollution and the planetary albedo, *Atmos. Environ.* (1967), 8, 1251–1256, [https://doi.org/10.1016/0004-6981\(74\)90004-3](https://doi.org/10.1016/0004-6981(74)90004-3), 1974.
- Vali, G.: Sizes of atmospheric ice nuclei, *Nature*, 212, 384–385, <https://doi.org/10.1038/212384a0>, 1966.
- 870 Vali, G., DeMott, P. J., Möhler, O., and Whale, T. F.: Technical note: a proposal for ice nucleation terminology, *Atmos. Chem. Phys.*, 15, 10263–10270, <https://doi.org/10.5194/acp-15-10263-2015>, 2015.
- Wagner, R., Möhler, O., Saathoff, H., Schnaiter, M., and Leisner, T.: High variability of the heterogeneous ice nucleation potential of oxalic acid dihydrate and sodium oxalate, *Atmos. Chem. Phys.*, 10, 7617–7641, <https://doi.org/10.5194/acp-10-7617-2010>, 2010.
- 875 Wagner, R., Möhler, O., Saathoff, H., Schnaiter, M., Skrotzki, J., Leisner, T., Wilson, T. W., Malkin, T. L., and Murray, B.: Ice cloud processing of ultra-viscous/glassy aerosol particles leads to enhanced ice nucleation ability, *Atmos. Chem. Phys.*, 12, 8589–8610, <https://doi.org/10.5194/ACP-12-8589-2012>, 2012.
- Wagner, R., Höhler, K., Huang, W., Kiselev, A., Möhler, O., Mohr, C., Pajunoja, A., Saathoff, H., Schiebel, T., Shen, X., and Virtanen, A.: Heterogeneous ice nucleation of α -pinene SOA particles before and after ice cloud processing, *J. Geophys. Res.: Atmos.*, 122, 4924–4943, <https://doi.org/10.1002/2016JD026401>, 2017.
- 880 Wang, B., Lambe, A., Massoli, P., Onasch, T., Davidovits, P., Worsnop, D., and Knopf, D.: The deposition ice nucleation and immersion freezing potential of amorphous secondary organic aerosol: pathways for ice and mixed-phase cloud formation, *J. Geophys. Res.*, 117, null, <https://doi.org/10.1029/2012JD018063>, 2012.
- 885 Wilson, T. W., Murray, B., Wagner, R., Möhler, O., Saathoff, H., Schnaiter, M., Skrotzki, J., Price, H., Malkin, T. L., Dobbie, S., and Al-Jumur, S. M. R. K.: Glassy aerosols with a range of compositions nucleate ice heterogeneously at cirrus temperatures, *Atmos. Chem. Phys.*, 12, 8611–8632, <https://doi.org/10.5194/ACP-12-8611-2012>, 2012.

- Wolf, M. J., Coe, A., Dove, L. A., Zawadowicz, M. A., Dooley, K., Biller, S. J., Zhang, Y., Chisholm, S. W., and Cziczo, D. J.: Investigating the heterogeneous ice nucleation of sea spray aerosols using prochlorococcus as a model source of marine organic matter, *Environ. Sci. Technol.*, 53, 1139–1149, <https://doi.org/10.1021/acs.est.8b05150>, 2019.
- 890 Wolf, M. J., Zhang, Y., Zawadowicz, M. A., Goodell, M., Froyd, K., Freney, E., Sellegri, K., Rösch, M., Cui, T., Winter, M., Lacher, L., Axisa, D., DeMott, P. J., Levin, E. J. T., Gute, E., Abbatt, J., Koss, A., Kroll, J. H., Surratt, J. D., and Cziczo, D. J.: A biogenic secondary organic aerosol source of cirrus ice nucleating particles, *Nat. Commun.*, 11, 4834, <https://doi.org/10.1038/s41467-020-18424-6>, 2020.
- 895 Wolf, M. J., Zhang, Y., Zhou, J., Surratt, J. D., Turpin, B. J., and Cziczo, D. J.: Enhanced ice nucleation of simulated sea salt particles with the addition of anthropogenic per- and polyfluoroalkyl substances, *ACS Earth Space Chem.*, 5, 2074–2085, <https://doi.org/10.1021/acsearthspacechem.1c00138>, 2021.
- Wyrzykowski, D., Hebanowska, E., Nowak-Wicz, G., Makowski, M., and Chmurzyński, L.: Thermal behaviour of citric acid and isomeric aconitic acids, *J. Therm. Anal. Calorim.*, 104, 731–735, <https://doi.org/10.1007/s10973-010-1015-2>, 2011.
- Zenker, J., Collier, K. N., Xu, G., Yang, P., Levin, E. J. T., Suski, K. J., DeMott, P. J., and Brooks, S. D.: Using depolarization to quantify ice nucleating particle concentrations: a new method, *Atmos. Meas. Tech.*, 10, 4639–4657, <https://doi.org/10.5194/amt-10-4639-2017>, 2017.
- 900 Zhang, C., Lu, M., Ma, N., Yang, Y., Wang, Y., Größ, J., Fan, Z., Wang, M., and Wiedensohler, A.: Hygroscopicity of aerosol particles composed of surfactant SDS and its internal mixture with ammonium sulfate at relative humidities up to 99.9%, *Atmos. Environ.*, 298, 119625, <https://doi.org/10.1016/j.atmosenv.2023.119625>, 2023.
- Zhang, Y., Nichman, L., Spencer, P., Jung, J. I., Lee, A., Heffernan, B. K., Gold, A., Zhang, Z., Chen, Y., Canagaratna, M. R., Jayne, J. T., Worsnop, D. R., Onasch, T. B., Surratt, J. D., Chandler, D., Davidovits, P., and Kolb, C. E.: The cooling rate- and volatility-dependent glass-forming properties of organic aerosols measured by broadband dielectric spectroscopy, *Environ. Sci. Technol.*, 53, 12366–12378, <https://doi.org/10.1021/acs.est.9b03317>, 2019.
- Zobrist, B., Marcolli, C., Pedernera, D. A., and Koop, T.: Do atmospheric aerosols form glasses, *Atmos. Chem. Phys.*, 8, 5221–5244, <https://doi.org/10.5194/ACP-8-5221-2008>, 2008.
- 910 Zobrist, B., Soonsin, V., Luo, B., Krieger, U., Marcolli, C., Peter, T., and Koop, T.: Ultra-slow water diffusion in aqueous sucrose glasses, *Phys. Chem. Chem. Phys. : Pccp*, 13 8, 3514–26, <https://doi.org/10.1039/c0cp01273d>, 2011.